Article

Current Biology

EGFR-dependent suppression of synaptic autophagy is required for neuronal circuit development

Graphical abstract

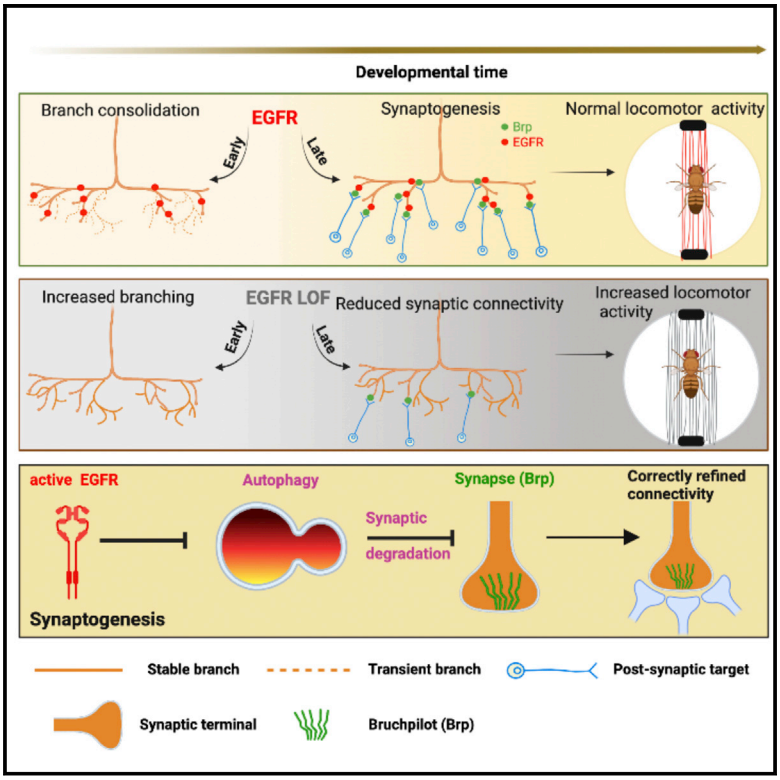

Highlights

- A critical developmental period of coupling axon branching to synaptogenesis
- Loss of EGFR activity uncouples axon branching from synapse formation
- EGFR activity suppresses autophagic degradation of presynaptic proteins
- Reduced autophagy during synaptogenesis is required for circuit connectivity

Authors

Suchetana B. Dutta, Gerit Arne Linneweber, Maheva Andriatsilavo, Peter Robin Hiesinger, Bassem A. Hassan

Correspondence

prh@zedat.fu-berlin.de (P.R.H.), bassem.hassan@icm-institute.org (B.A.H.)

In brief

Using the development of the fruit fly *Drosophila melanogaster* brain as a model system, Dutta et al. identify a critical developmental period during which coupling axon branching to synaptic degradation is required for neural circuit formation. This coupling relies on EGFR-dependent restriction of local synaptic degradation.

Dutta et al., 2023, Current Biology *33*, 1–16
February 6, 2023
https://doi.org/10.1016/j.cub.2022.12.039

CellPress

Current Biology

CellPress

Article

EGFR-dependent suppression of synaptic autophagy is required for neuronal circuit development

Suchetana B. Dutta,[1,2,3] Gerit Arne Linneweber,[2] Maheva Andriatsilavo,[1,2,3] Peter Robin Hiesinger,[2,*] and Bassem A. Hassan[1,2,3,4,5,*]

[1]Institut du Cerveau-Paris Brain Institute (ICM), Sorbonne Université, Inserm, CNRS, Hôpital Pitié Salpêtrière, 75013 Paris, France
[2]Division of Neurobiology, Free University of Berlin, 14195 Berlin, Germany
[3]Einstein-BIH, Charité Universitätsmedizin, 10117 Berlin, Germany
[4]Twitter: @TheHassanLab
[5]Lead contact
*Correspondence: prh@zedat.fu-berlin.de (P.R.H.), bassem.hassan@icm-institute.org (B.A.H.)
https://doi.org/10.1016/j.cub.2022.12.039

SUMMARY

The development of neuronal connectivity requires stabilization of dynamic axonal branches at sites of synapse formation. Models that explain how axonal branching is coupled to synaptogenesis postulate molecular regulators acting in a spatiotemporally restricted fashion to ensure branching toward future synaptic partners while also stabilizing the emerging synaptic contacts between such partners. We investigated this question using neuronal circuit development in the *Drosophila* brain as a model system. We report that epidermal growth factor receptor (EGFR) activity is required in presynaptic axonal branches during two distinct temporal intervals to regulate circuit wiring in the developing *Drosophila* visual system. EGFR is required early to regulate primary axonal branching. EGFR activity is then independently required at a later stage to prevent degradation of the synaptic active zone protein Bruchpilot (Brp). Inactivation of EGFR results in a local increase of autophagy in presynaptic branches and the translocation of active zone proteins into autophagic vesicles. The protection of synaptic material during this later interval of wiring ensures the stabilization of terminal branches, circuit connectivity, and appropriate visual behavior. Phenotypes of EGFR inactivation can be rescued by increasing Brp levels or downregulating autophagy. In summary, we identify a temporally restricted molecular mechanism required for coupling axonal branching and synaptic stabilization that contributes to the emergence of neuronal wiring specificity.

INTRODUCTION

Proper neuronal wiring is critical for brain function and relies on a robust and stereotyped neuronal connection.[1–3] Axon branching and synapse formation are regulated in space and time through local probabilistic events like filopodial growth and retraction, local protein recycling and degradation, cytoskeletal polymerization and depolymerization, or stochastic synaptic seeding to ensure the specificity of neuronal connectivity.[4–7] This raises the question of how such probabilistic developmental events are orchestrated in space and time to ensure the robustness of neuronal circuits and how individual axons and their branches locally pattern to connect to postsynaptic targets.

During late neuronal development, after an initial phase of exploratory axonal branching, interdependence between synapse formation and branching dynamics plays a key role in the selection of future synaptic partners.[8–10] This ''synaptotropic'' iterative ensures the reproducibility of wiring patterns and might itself act as a limiting factor to prevent excessive branch growth and allow a stable adult pattern.[11] These necessitate the existence of local molecular mechanisms that act in a temporal specific manner to couple axonal branching dynamics to synapse formation. The identity and mode of action of such temporal molecular coupling events are poorly understood.

The formation of a stable synaptic contact is a function of the equilibrium between synaptic seeding and synaptic degradation as shown during developmental pruning processes.[12] Synapse elimination is an important cellular phenomenon which fine tunes neural circuitry[13] especially during post-natal experience-dependent plasticity known as ''critical period.''[14] Interestingly, the existence of prenatal synapse pruning known as ''precritical period'' plasticity in the visual cortex[15] suggests that genetically encoded events may define critical developmental intervals of synaptic consolidation and elimination prior to the onset of experience-dependent plasticity. The timing, role, and molecular regulation of such developmental events are unknown.

Autophagy is a key cellular homeostasis mechanism, which also plays a role in brain development.[16] Its loss results in morphological and functional presynaptic organization defects as shown in the mouse cochlear ribbon synapse[17] and *Drosophila* mushroom body and photoreceptor neurons.[18,19] At the *Drosophila* neuromuscular junction, disruption of autophagy reduces its size, whereas induction of autophagy increases synaptic boutons and neuronal branches.[20] Autophagy

Please cite this article in press as: Dutta et al., EGFR-dependent suppression of synaptic autophagy is required for neuronal circuit development, Current Biology (2022), https://doi.org/10.1016/j.cub.2022.12.039

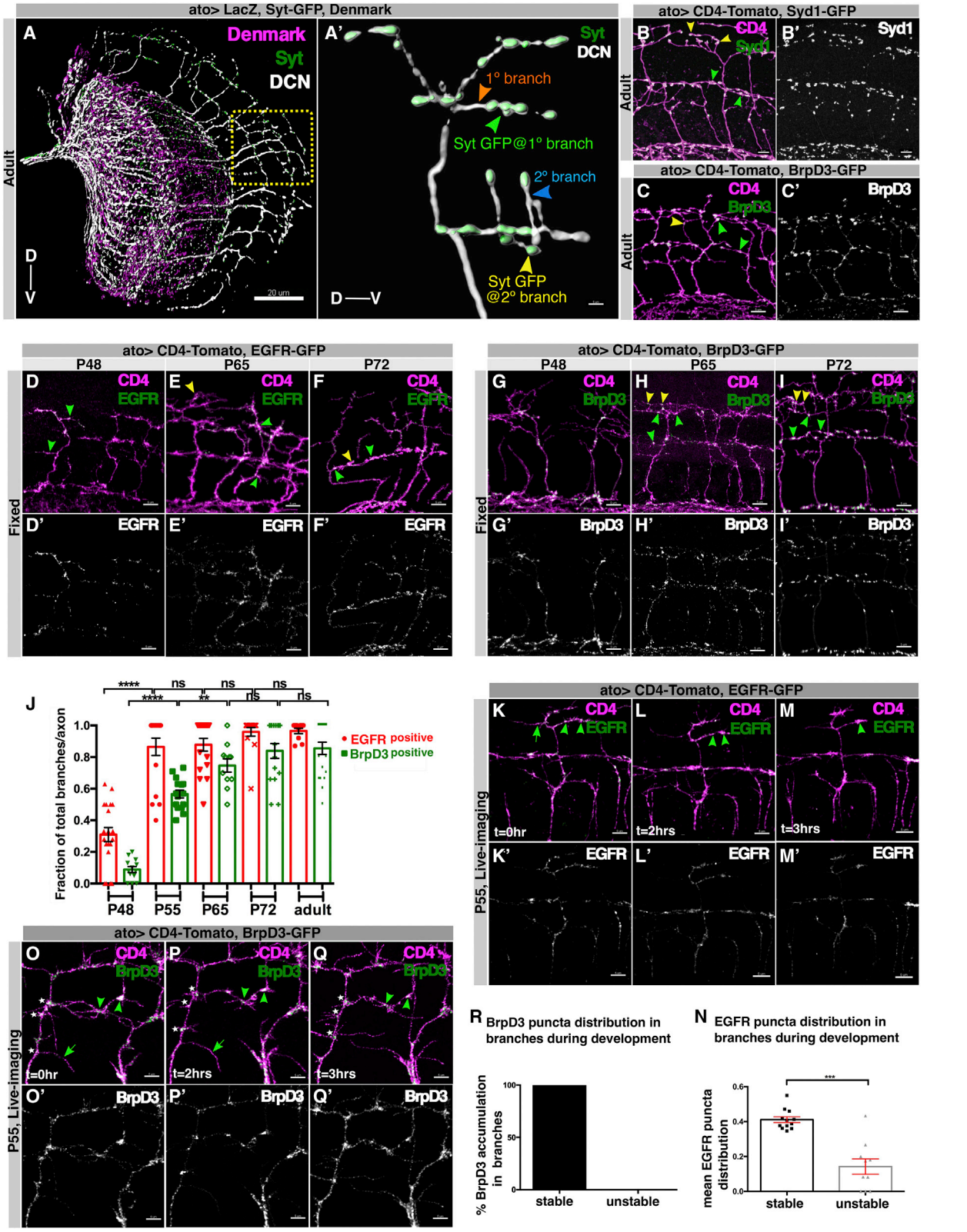

Figure 1. Spatiotemporal correlation of the molecular mechanisms of branching and synapse formation during development

(A) Adult stereotypic projection pattern of DCNs driven by *atoGal4-14a* labeled with LacZ (white), dendritic arborizations marked by Denmark (magenta), and presynaptic sites marked by Syt-GFP (green). *atoGal4-14a* is used in all the following experiments unless otherwise stated. Yellow box represents region of

(legend continued on next page)

Please cite this article in press as: Dutta et al., EGFR-dependent suppression of synaptic autophagy is required for neuronal circuit development, Current Biology (2022), https://doi.org/10.1016/j.cub.2022.12.039

deficiency also causes dendritic spine pruning defects and autism-like social behaviors in a mouse model.[21] Presynaptic sites are zones of autophagosome biogenesis that have been linked to synaptic plasticity[22,23] and local autophagy may also play a role in positioning axonal branches.[24] How axonal branch growth and refinement are molecularly coupled to synapse formation and pruning in space and time during neuronal circuit wiring is not well understood.

In order to molecularly dissect the link between axonal branching and synapse formation during neuronal circuit development, we used the higher order neurons called dorsal cluster neurons (DCNs)[25] from the *Drosophila* visual system. A subset of DCNs (the medulla-innervating DCNs [M-DCNs]) projects their axons to a distal visual neuropil: the medulla, where they form a stereotypical fan-shaped branching pattern.[26,27] M-DCN wiring patterns determine visual object orientation behavior in flies.[28] We have previously shown that a local asymmetric localization and recycling of the epidermal growth factor receptor (EGFR) as well as its activation in M-DCN axonal filopodia during development were linked to actin polymerization and filopodial dynamics to regulate the establishment the presynaptic M-DCN branches final pattern.[29]

In this study, we identified the molecular and cellular mechanisms underlying interdependent branching and synapse formation of M-DCN axons and its consequences on circuit wiring and behavior. We found that EGFR activity is required at two distinct temporal intervals. First, an early actin-dependent interval establishes primary axonal branches where presynaptic material accumulates. Then, EGFR function prevents autophagic degradation of the presynaptic active zone (AZ) scaffold protein Bruchpilot (Brp) stabilizing synaptic contacts. We conclude that a temporal sequence of local molecular interactions coordinated by EGFR signaling ensures the coupling between progressive axonal branch refinement and stabilization of the presynaptic AZ and thus contributes to axon-specific connectivity.

RESULTS

Spatiotemporal correlation of the molecular mechanisms of branching and synapse formation during development

To investigate the relationship between terminal axon branching and synapse formation at high spatiotemporal resolution, we used the M-DCNs as a model. M-DCNs axons form stable terminal primary and secondary presynaptic branches in several posterior medulla layers[29] (Figures 1A and 1A′). Each M-DCN axon forms an average of 4.5 primary branches and 1.5 secondary branches per axon (Figure S1G) and contains presynaptic sites marked by the presynaptic and AZ proteins: synaptotagmin (Syt), Syd1, and Brp (Figures 1A, 1A′, 1C, and 1C′). We have previously shown that the number of M-DCN axonal presynaptic branches is regulated by local EGFR activity[29] between 48 and 72 h of pupal development (P48–P72 at 25°C).

To investigate the spatiotemporal pattern of synapse formation in the context of axonal branching, we quantified the order of appearance of EGFR (EGFR GFP), Syd1 (Syd1-GFP), and Brp (BrpD3-GFP) in M-DCN branches between P48 and P72 using well-established reporters of the localization of the endogenous proteins that show no known overexpression phenotypes.[29–31] At P48, ~60% of all the branches contained Syd1-GFP, ~30% contained EGFR GFP, but less than 10% contained BrpD3 puncta (Figures 1D, 1D′, 1G, 1G′, 1J, S1A, S1A′, and S1D). Between P55 and P65, ~90% contained EGFR GFP and Syd1-GFP puncta, while the number of branches with BrpD3 puncta increased from ~50% to ~75% (Figures 1E, 1E′, 1H, 1H′, 1J, S1B, S1B′, and S1D). By P72, all three proteins have reached adult levels (Figures 1B–1C′, 1F, 1F′, 1I, 1I′, 1J, 2A, 2A′, S1C, and S1D). Thus, Syd1 entered DCN axons around P40 (Figures S1E–S1F′) followed by EGFR and then Brp.

To reveal the dynamics of this process, we lived imaged and quantified the trafficking of BrpD3-GFP, Syd-1-GFP, and EGFR GFP in *ex vivo* cultures at P55 when all three proteins are present in branches *in vivo*. We specifically quantified discrete clusters

interest where DCN axons form ladder-like branches as shown in (A′), higher resolution with primary (orange arrowhead) and secondary branches (blue arrowhead) harboring Syt-GFP (green) puncta in both primary (green arrowhead) and secondary (yellow arrowhead) terminals. Similar annotations are used in all the following figures to denote primary branch (orange arrowhead), secondary branch (blue arrowhead), and respective protein harboring primary (green arrowhead) or secondary (yellow arrowhead) branch terminals that have been quantified.

(B and C) Adult DCN branches (magenta) are associated with clusters of early synaptic seeding factor, marked with Syd1 GFP (green) (B and B′), and late active zone (AZ) protein Brp, marked with BrpD3 GFP (green) (C and C′).

(D–I) Temporal order of recruitment of EGFR GFP (green) and BrpD3 GFP (green) in the DCN branches (magenta) during development, P48 (D, D′, G, and G′), P65 (E, E′, H, and H′) and P72 (F, F′, I, and I′), showing EGFR enters the branches before Brp.

(J) Quantification showing the fraction of all branches per axon recruiting EGFR GFP (red data points) and BrpD3 GFP (green data points) during development from fixed samples. n = 20 axons, N = 6 individuals at P48 (EGFR); n = 17 axons, N = 5 individuals at P48 (BrpD3); n = 17 axons, N = 5 individuals at P55 (EGFR); n = 17 axons, N = 5 individuals at P55 (BrpD3); n = 17 axons, N = 5 individuals at P65 (EGFR); n = 14 axons, N = 5 individuals at P65 (BrpD3); n = 15 axons, N = 5 individuals at P72 (EGFR); n = 16 axons, N = 5 individuals at P72 (BrpD3); n = 11 axons, N = 4 individuals in adult (EGFR); and n = 20 axons, N = 7 individuals in adult (BrpD3). Mann-Whitney test; ****$p < 0.0001$, $^{ns}p = 0.8124$, $^{ns}p = 0.7934$, $^{ns}p = 0.4932$.

(K–M and O–Q) *Ex vivo* imaging of EGFR GFP (K–M′) and BrpD3 GFP (O–Q′) in the DCN branches (magenta) during development shows EGFR GFP (green) asymmetrically localizes in the DCN branches—stable branches with higher proportion of EGFR punctas (arrow) compared with unstable branches (arrowhead) (K–M′)—whereas late AZs marked by BrpD3 GFP (green) accumulate only in stable branches (arrow), while being excluded from unstable branches (arrowhead) (O–Q′).

(N) Quantification of mean EGFR GFP puncta normalized to branch length in stable (black bar) versus unstable primary branches (gray bar) in *ex vivo* cultures during development. N = 12 for stable branches and N = 10 for unstable branches for 3 individuals, Mann-Whitney test, ***$p = 0.0003$.

(R) Quantification of percentage of BrpD3 GFP puncta accumulation in stable (black bar) versus unstable primary branches during development. N = 10 for stable branches and N = 15 for unstable branches for 3 individuals.

Error bars denote mean ± SEM; scale bar represents 5 μm except (A), which represents 20 μm.

See also Figure S1, Video S1, and Data S1.

Please cite this article in press as: Dutta et al., EGFR-dependent suppression of synaptic autophagy is required for neuronal circuit development, Current Biology (2022), https://doi.org/10.1016/j.cub.2022.12.039

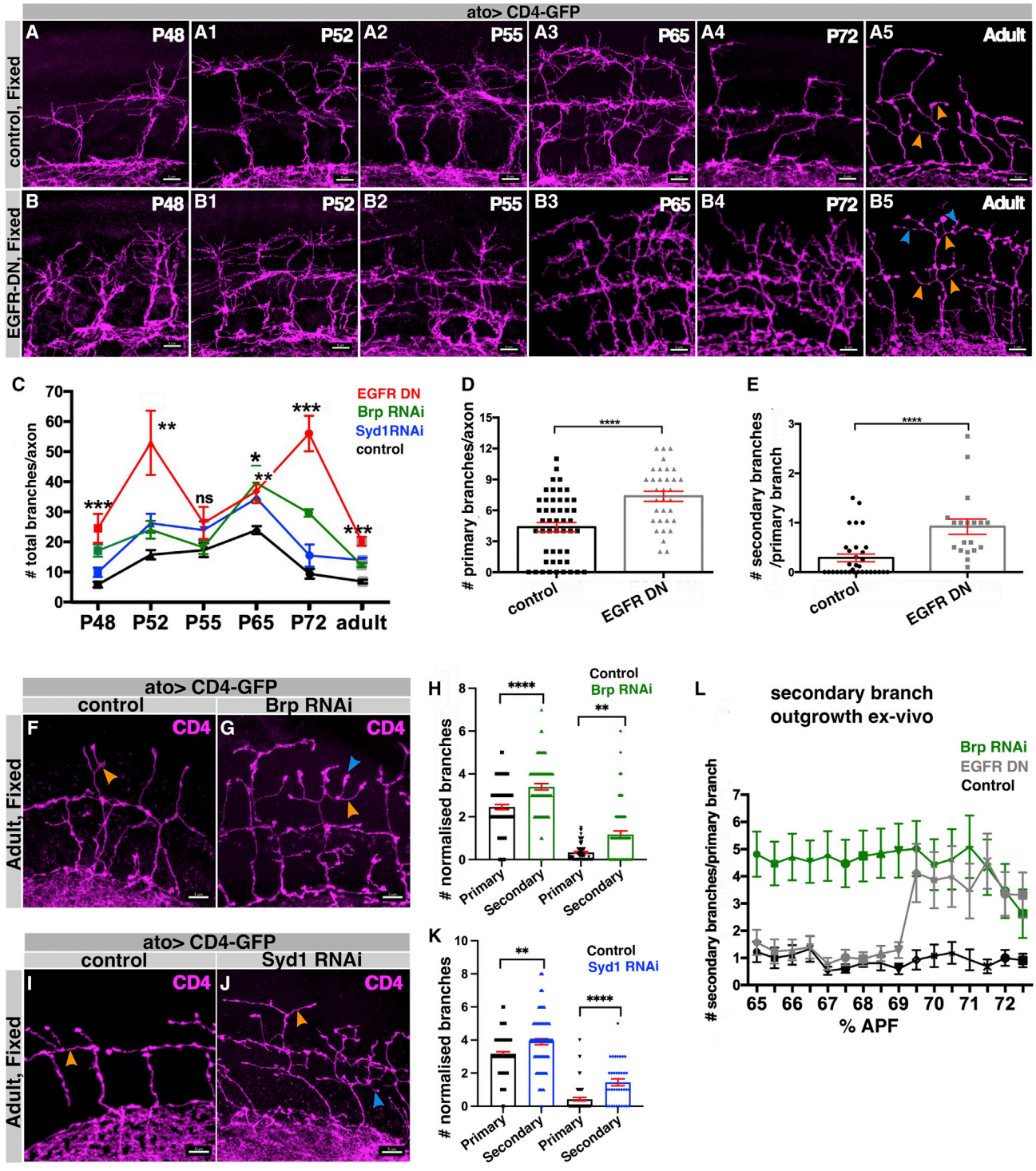

Figure 2. Synapse formation is required for terminal branch patterning

(A) DCN axonal branch progression (magenta) during development in control brains reveals an increase in branching complexity from early to mid-pupal stage: P48 (A), P52 (A1), P55 (A2), and P65 (A3). Branch refinement occurs from mid- to late-pupal development: P65 (A3), P72 (A4), and adult (A5).

(B) Surprisingly, EGFR-DN-expressing DCNs show dysregulation of branch refinement process with branching peaks at two phases of development: first from P48 to P55 (B–B2) and later from P65 to adult (B3–B5).

(C) Quantification showing overall branch refinement progression (mean of the total number of branches per axon) during development in EGFR-DN (red), Brp RNAi (green), and Syd1 RNAi (blue) compared with control (black). For P48, N = 8 individuals for control and N = 6 individuals for EGFR-DN, Brp RNAi, and Syd1 RNAi. For P52, N = 6 individuals for control and N = 5 individuals for EGFR-DN, Brp RNAi, and Syd1 RNAi. For P55, N = 6 individuals for control and N = 5 individuals for EGFR-DN, Brp RNAi, and Syd1 RNAi. For P65, N = 6 individuals for control and EGFR-DN and N = 5 individuals for Brp RNAi and Syd1 RNAi. For

(legend continued on next page)

Please cite this article in press as: Dutta et al., EGFR-dependent suppression of synaptic autophagy is required for neuronal circuit development, Current Biology (2022), https://doi.org/10.1016/j.cub.2022.12.039

(henceforth "puncta") of the respective synaptic molecules in stable versus unstable primary branch populations. We defined any branches that were present during the entire imaging session (~8 h) as "stable," and as "unstable" any branches that retracted without re-growing during that time window. Whereas Syd1 entered in all branches regardless of stability (Figures S1H–S1K; Video S1), EGFR accumulated preferentially, but not exclusively, in stable branches compared with unstable branches (Figures 1K–1N; Video S1). While Brp accumulated at the base of primary branches on the axon shaft, it exclusively accumulated in stable branches. Branches without BrpD3 puncta during development failed to stabilize, suggesting that AZ maturation is a prerequisite for branch stabilization (Figures 1O–1R; Video S1). Taken together, our spatial and temporal analyses of *in vivo* live imaging data suggest that almost all branches are synapse competent (contain Syd1 early), but only the fraction that accumulates both EGFR and Brp is stabilized to contain future synaptic AZs.

Synapse formation is required for branch patterning

To investigate the molecular interdependence of axon branching and synapse formation, we inactivated EGFR, Syd1, or Brp and examined branch development *in vivo* starting from P48. In controls, M-DCN axon branch numbers increased gradually from P48, reached their maxima at P65 and then declined to reach adult branch numbers at P72 (Figures 2A–2A5 and 2C). Brp entry preceded this gradual branch refinement between P65 and P72 (Figures 1J and 1R), suggesting a link between synapse formation and branch stabilization. As previously shown, EGFR inactivation using a well-established dominant-negative transgene (EGFR-DN)[32] resulted in an increase in the total number of primary and secondary branches in adults (Figures 2B5 and 2C). Surprisingly, the temporal branch dynamic pattern showed a bi-phasic pattern of growth and pruning from P48 to P55 and from P55 to adult (Figures 2B and 2C) with two maxima at P52 and P72, which ultimately led to increased primary and secondary branching in adults (Figures 2C–2E). These data suggest that EGFR is required during two distinct temporal intervals for DCN branch pruning.

Suppression of EGFR function causes early pruning defects of primary branches between P48 and P55 through an actin-dependent mechanism.[29] We therefore asked whether changes in actin dynamics could explain branching phenotypes during both early and late phases of growth and pruning upon EGFR inactivation. RNAi knockdown of several cytoskeletal regulators resulted in an increase of primary branches, but not of secondary branches (Figures S1L–S1Q). To test whether the increase in adults secondary branches arises from the second growth/pruning phase (P65–P72) (Figure 2C), we performed live imaging of axonal branching dynamics specifically during this second phase. Indeed, suppression of EGFR function led to a late surge of secondary branch outgrowth between P65 and P72 that was not observed in wild type (Figure 2L; Video S2). This suggests that branch regulation during the second growth/pruning EGFR-sensitive phase is mechanistically distinct from the first phase and coincides with Brp recruitment into stable primary branches.

We then asked whether loss of proteins required to form functional synapses influences axonal branching during that second developmental interval. We knocked down Syd-1 and Brp specifically in DCNs throughout development using Syd1 RNAi and Brp RNAi (line B3,C8).[33] Similar to EGFR inactivation, both conditions resulted in an increase in the numbers of primary and secondary branches in adults suggesting defects in branch pruning (Figures 2C and 2F–2K). These defects only occurred during the second EGFR-sensitive phase between P65 and P72 (Figure 2C). Live imaging revealed secondary branch outgrowth throughout the P65–P72 time window upon Brp RNAi (Figure 2L; Video S3) and a continued exploratory growth/retraction mode of branches in adult brains (Video S3). Thus, defective synapse formation results in continued synaptogenic exploration of branches from late development onward, suggesting that synapse formation is required for branch stabilization. Altogether, these observations suggest a temporally restricted link among EGFR activity, branching dynamics, and synapse formation during a late developmental interval of neural circuit wiring.

P72, N = 6 individuals for control and Syd1 RNAi and N = 5 individuals for EGFR-DN and Brp RNAi. For adults, N = 7 individuals for control, EGFR-DN, Brp RNAi, and Syd1 RNAi. Kruskal-Wallis and Dunn's as post hoc test; ***p = 0.0004 (P48), **p = 0.0016 (P52), ^{ns}p = 0.1835 (P55), **p = 0.0091 (P65), ***p = 0.0004 (P72), and ***p = 0.0005 (adult). Detailed statistics in Data S1.

(D) Quantification showing increased primary branch number per axon in EGFR-DN (gray) expressing DCNs compared with genetic control (black) in adults. N = 49 axons, 11 individuals for control; N = 33 axons, 9 individuals for EGFR-DN; t test, ****p < 0.0001.

(E) Quantification showing increased secondary branch number per primary branch in EGFR-DN (gray) expressing DCNs compared with control (black) in adults. n = 32 primary branches, N = 6 individuals for control; n = 19 primary branches, N = 6 individuals for EGFR-DN; t test, ****p < 0.0001. Error bars denote mean ± SEM.

(F, G, I, and J) Adult axonal branch pattern (magenta) upon knocking down Brp (F and G) and Syd1 (I and J) specifically in DCNs compared with their genetic controls.

(H) Adult quantification showing increased number of primary branches (normalized to total number of axons) and secondary branches (normalized to total number of primary branches) in Brp B3,C8 RNAi (green) compared with control (black). n = 49 axons, N = 12 individuals for control; n = 38 axons, N = 11 individuals for Brp B3,C8 RNAi in primary branch quantification. n = 54 branches, N = 9 individuals in control; n = 60 branches, N = 10 individuals for Brp B3,C8 RNAi in secondary branch quantification. Mann-Whitney test, ****p < 0.0001, **p = 0.0011.

(K) Adult quantification showing similar increase in primary (normalized to total number of axons) and secondary branch (normalized to total number of primary branches) number of adult DCNs in Syd1 RNAi (blue) compared with control (black). n = 92 axons, N = 15 individuals for control; n = 90 axons, N = 15 individuals for Syd1 RNAi in primary branch quantification. n = 66 branches, N = 10 individuals in control; n = 36 branches, N = 7 individuals in Syd1-RNAi in secondary branch quantification. Mann-Whitney test, **p = 0.0011, ****p < 0.0001.

(L) Quantification of the temporal outgrowth of secondary branches (secondary branch number normalized to number of primary branches) in every 30-min interval between P65 and P72 *ex vivo* cultures in Brp B3,C8 RNAi (green) or EGFR-DN (gray) compared with control (black). n = 29 branches, N = 3 individuals for Brp B3,C8 RNAi (green); n = 20 branches, N = 3 individuals for EGFR-DN (gray); and n = 18 branches, N = 3 individuals for control (black). Error bars denote mean ± SEM; scale bar represents 5 μm.

See also Figure S1, Videos S2 and S3, and Data S1.

Please cite this article in press as: Dutta et al., EGFR-dependent suppression of synaptic autophagy is required for neuronal circuit development, Current Biology (2022), https://doi.org/10.1016/j.cub.2022.12.039

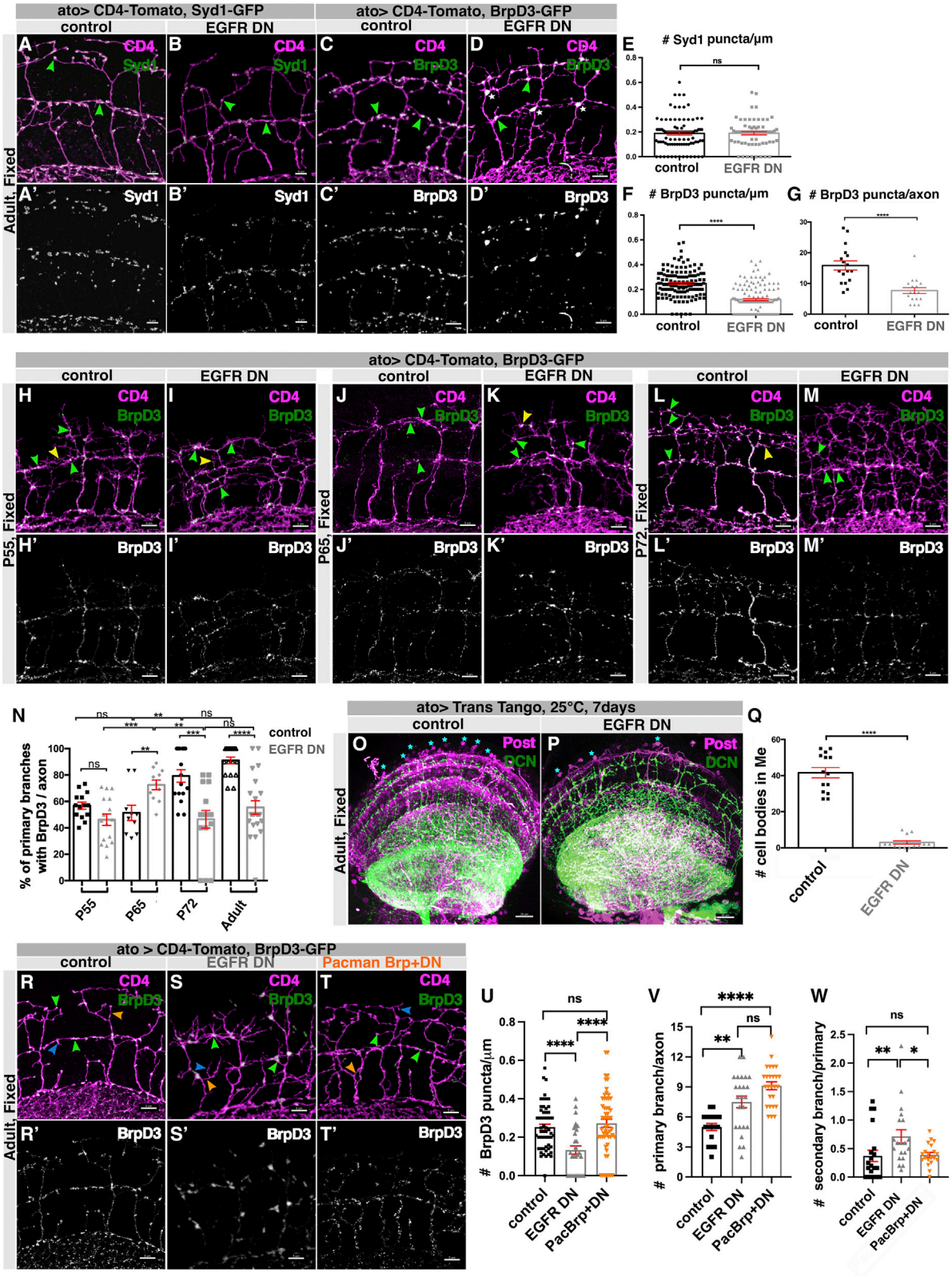

Figure 3. EGFR is required for Brp stabilization in terminal branches

(A–D) Adult DCN axon branches contain early seeding factor Syd1-GFP, which is unaffected in EGFR-DN (A–B′), while late AZ marker BrpD3-GFP reduces drastically in the branches where they accumulate in larger volumes (white asterisks) in EGFR-DN (C–D′).

(legend continued on next page)

Please cite this article in press as: Dutta et al., EGFR-dependent suppression of synaptic autophagy is required for neuronal circuit development, Current Biology (2022), https://doi.org/10.1016/j.cub.2022.12.039

EGFR is required for Brp stabilization and synaptic connectivity

To investigate the cross-regulation between EGFR activity and synapse formation, we asked whether and how Syd1, EGFR, and Brp interact genetically to establish M-DCN connectivity. Syd1 is known to recruit Brp to future presynaptic sites.[31,34] However, knockdown of Syd1 or Brp had no effect on the distribution or levels of EGFR in adult branches (Figures S2A, S2A′, S2C, S2C′, and S2D). Conversely, inactivation of EGFR did not affect the number of Syd1 puncta distribution in the branches (Figures 3A–3B′ and 3E). This suggests that EGFR and Syd1 act in parallel during synapse formation. In contrast, suppression of EGFR activity resulted in a significant decrease of AZs based on a reduction of the BrpD3-GFP marker, which colocalizes with endogenous Brp (Figures S2E–S2F′). The BrpD3 adult distribution changes from 0.22 puncta per μm in control to 0.1 per μm in EGFR-DN (Figures 3C–3D′ and 3F). This loss of BrpD3 distribution per branch length unit corresponds to a 2.5-fold decrease in the total number of BrpD3 puncta from ~15 to ~6.5 per axon. It was accompanied by a redistribution from numerous small puncta at presynaptic sites into a few large BrpD3 aggregates (Figures 3C–3D′ and 3G), an indicator of endogenous AZs loss in DCNs.[35]

Given that EGFR enters branches before Brp, we asked when EGFR was required for the presence of Brp in branches. We examined the recruitment and accumulation of BrpD3-GFP in M-DCN axons and primary branches over time. Inactivation of EGFR did not interfere with the initial recruitment of BrpD3-GFP at P55 (Figures 3H–3I′ and 3N). At P65, where EGFR inactivation led to an increase in branch number, it also caused an increase in the number of BrpD3 puncta (Figures 3J–3K′ and 3N). In contrast, we observed a significant decrease of BrpD3 levels starting at P72 and continuing into adults (Figures 3H–3N). To examine the temporal dynamics of the gradual loss of BrpD3 after initial recruitment, we performed live imaging and calculated the stability of BrpD3-GFP puncta in branches during synaptogenesis. Brp puncta stability was tracked for 2 h in *ex vivo* cultures at P65 and P72. We classified puncta as stable if they were present throughout tracking, or as unstable if they disappeared at any point during the tracking. Between P65 and P67, 82% of Brp puncta were stable in control DCNs compared with 57% in EGFR-DN DCNs. Between P72 and P74, 93% of Brp puncta became stable in controls compared with 76% in EGFR-DN expressing DCNs (Figure S2G; Video S4). Because Brp acts as a scaffold protein for AZ formation,[36] these suggest that suppression of EGFR activity reduces the stability of AZs during late brain development. To further validate the AZ reduction, we analyzed Unc13a protein, which closely associates with Brp.[37] Suppression of EGFR function leads to a significant reduction of Unc13a puncta in adult axonal branches and to an accumulation along the axonal shaft, similar to Brp (Figures S2H–S2J). We conclude that EGFR activity is required to maintain AZs in axonal branches.

EGFR inactivation causes an increase in primary and secondary axon branches, yet simultaneously causes a sharp decrease of the AZ numbers. What is the impact of these seemingly opposing changes on DCN postsynaptic connectivity and circuit wiring? To test this, we first determined the DCN connectome in the medulla. We used the anterograde transsynaptic method for target tracing approach "*trans*-Tango," which labels all the postsynaptic targets in an unbiased manner without required prior knowledge of cell types.[38] We used stringent conditions (STAR Methods) to optimize sparse labeling of postsynaptic targets (Figures S2K and S2L). M-DCNs connect to a large variety of

(E) Quantification showing unaffected distribution of Syd1-GFP puncta number normalized to axon branch length in control (black) versus EGFR-DN (gray) in adults. n = 93 branches, N = 15 individuals for control and n = 66 branches, N = 11 individuals for EGFR-DN; t test, p = 0.6688.
(F) Quantification showing reduction in distribution of BrpD3-GFP puncta number normalized to axon branch length in control (black) versus EGFR-DN (gray) in adults. n = 124 branches, N = 20 individuals for control and EGFR-DN, t test, ****p < 0.0001.
(G) Adult quantification of the total number of BrpD3-GFP puncta per axon in control (black) versus EGFR-DN (gray). n = 17 axons, N = 5 individuals for control and EGFR-DN. Mann-Whitney test; ****p < 0.0001.
(H–M) Recruitment of BrpD3-GFP puncta (green) in developing DCN branches labeled by CD4-tomato (magenta) in fixed samples during different stages of pupal development in control versus EGFR-DN: P55 (H–I′), P65 (J–K′), and P72 (L–M′).
(N) Quantification showing percentage of BrpD3-GFP-positive DCN branches per axon during development in control (black) versus EGFR-DN (gray). n = 14 axons, N = 5 individuals for control; P55, n = 16 axons, N = 5 individuals for EGFR-DN; P55, n = 14 axons, N = 5 individuals for control; P65, n = 11 axons, N = 4 individuals for EGFR-DN; P65, n = 16 axons, N = 5 individuals for control; P72, n = 18 axons, N = 6 individuals for EGFR-DN, n = 18 axons, N = 6 individuals for control; adult, n = 22 axons, N = 7 individuals for EGFR-DN; adult. Kruskal-Wallis and Dunn's as post hoc test; ****p < 0.0001.
(O and P) Labeling of postsynaptic partners (magenta) of adult DCNs (green) in the medulla (white arrowheads) using *trans*-Tango at 25°C for 7 days showing reduced connectivity in EGFR-DN (P) compared with control (O).
(Q) Quantification showing reduced postsynaptic cell body number in medulla in control (black) versus EGFR-DN (gray) in adult DCNs at 25°C for 7-day-old adults. N = 14 individual optic lobes for control and EGFR-DN; ****p < 0.0001, Mann-Whitney test.
(R–T) Rescue of BrpD3 GFP (green) puncta and secondary branches in adult DCNs labeled by uas-CD4 tomato (magenta) with increased gene copy number of Brp (Pacman Brp) in EGFR-DN background (T and T′) back to control level (R and R′) compared with EGFR-DN alone (S and S′) in adults.
(U) Adult quantification showing the rescue of BrpD3 GFP puncta normalized to individual axon branch length in Pacman Brp + $EGFR^{DN}$ (orange) back to control (black) level compared with EGFR-DN (gray). n = 58 primary branches, N = 9 individuals for control; n= 30 primary branches, N = 5 individuals for EGFR-DN; n = 56 primary branches, N = 9 individuals for Pacman Brp+ EGFR-DN. Kruskal-Wallis and Dunn's as post hoc test; ****p < 0.0001.
(V) Quantification showing no rescue of adult primary branch number per axon in Pacman Brp + EGFR-DN (orange) back compared with EGFR-DN (gray). n = 18 axons, N = 6 individuals for control; n = 24 axons, N = 7 individuals for EGFR-DN; n = 26 axons, N = 7 individuals for Pacman Brp+ EGFR-DN. Kruskal-Wallis and Dunn's as post hoc test; ****p < 0.0001.
(W) Quantification showing rescue of adult secondary branch number per primary branch in Pacman Brp + EGFR-DN (orange) back to control (black) level compared with EGFR-DN (gray). n = 20 primary branches, N = 4 individuals for control, EGFR-DN and Pacman Brp + EGFR-DN. Kruskal-Wallis and Dunn's as post hoc test; **p = 0.0007.
Error bars denote mean ± SEM; scale bar represents 5 μm, except for (O) and (P), where it represents 20 μm.
See also Figures S2 and S3, Video S4, and Data S1.

Please cite this article in press as: Dutta et al., EGFR-dependent suppression of synaptic autophagy is required for neuronal circuit development, Current Biology (2022), https://doi.org/10.1016/j.cub.2022.12.039

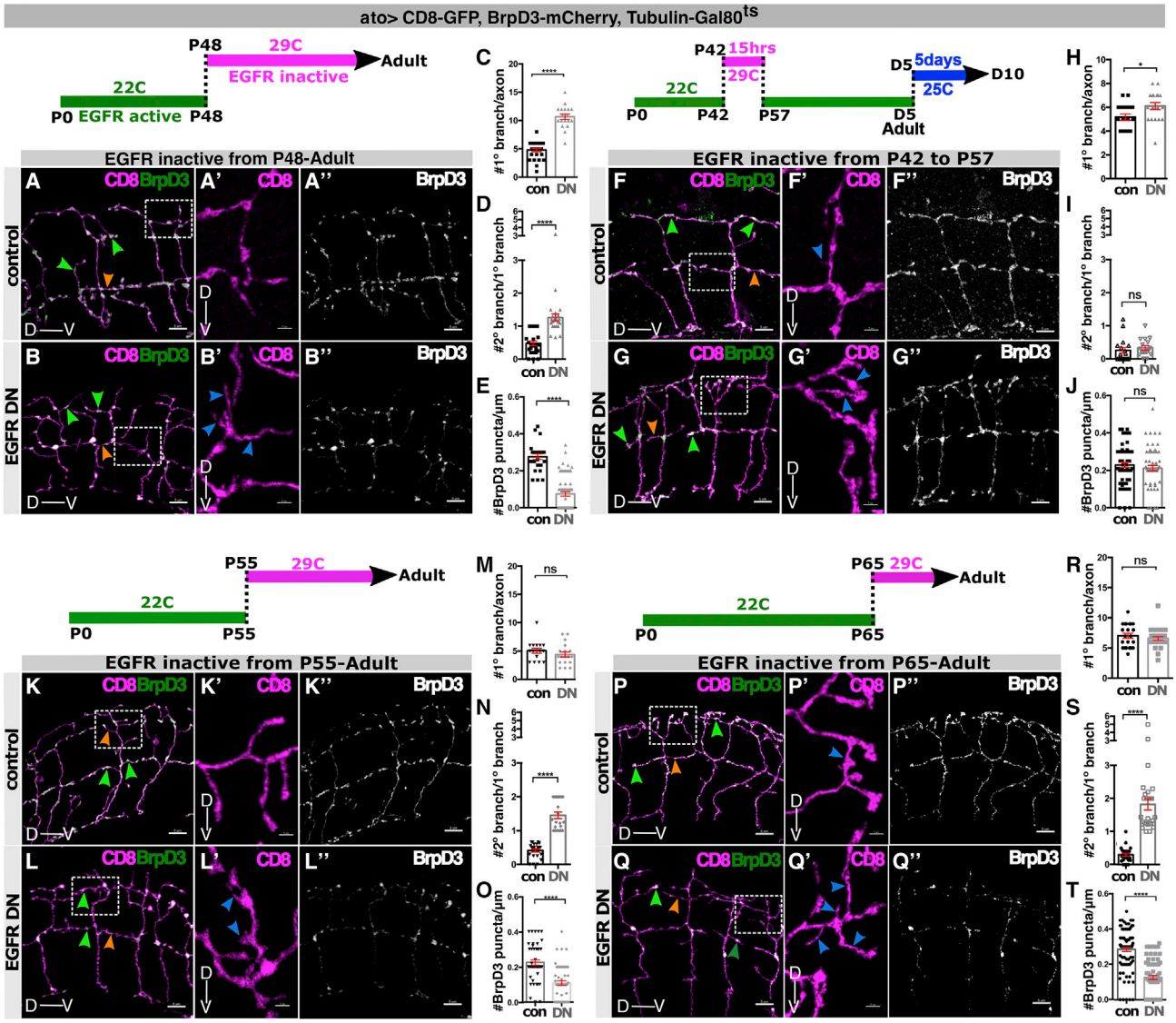

Figure 4. Temporal requirement of EGFR activity in synapse formation and primary branch consolidation

Adult DCN branch morphology labeled by uas-CD8 GFP (magenta) and AZs marked by uas-BrpD3-mCherry (green). EGFR is active when shifted to 22°C (green bar) but inactive when shifted to 29°C (magenta bar). We inactivated EGFR temporally by shifting the Gal80^{ts} construct to 29°C during different developmental time intervals and analyzed young adults unless otherwise stated. White squares represent regions of higher magnification.

(A and B) Lack of EGFR activity from P48 throughout development results in more primary (A and B) and secondary branching (A′ and B′) with reduced BrpD3-mCherry puncta number (A″ and B″) in adult DCN branches compared with control.

(C) Quantification showing increased primary branch number per axon in control (black) versus EGFR-DN (gray). n = 25 axons, N = 7 individuals for control; n = 26 axons, N = 7 individuals for EGFR-DN. Mann-Whitney test; ****p = 0.0001.

(D) Quantification showing increased secondary branches per primary branch in control (black) versus EGFR-DN (gray). n = 25 primary branches, N = 4 individuals for control and n = 22 primary branches, N = 4 individuals for EGFR-DN. Mann-Whitney test; ****p < 0.0001.

(E) Quantification showing decreased BrpD3-mCherry puncta per unit branch length in control (black) versus EGFR-DN (gray). n = 25 branches, N = 5 individuals for control and n = 66 branches, N = 7 individuals for EGFR-DN. Mann-Whitney test; ****p = 0.0001.

(F and G) Lack of EGFR activity only between P42 and P57 during development results in more primary branching (F and G) with no effect on secondary branching (F′ and G′) or BrpD3-mCherry puncta localization (F″ and G″) in adult DCNs compared with control. The young adults (D5) were shifted to 25°C for 5 days for transgene expression prior to analyses.

(H) Quantification showing increased primary branch number per axon in control (black) versus EGFR-DN (gray). n = 17 axons, N = 5 individuals for control and n = 18 axons, N = 5 individuals for EGFR-DN. Mann-Whitney test; *p = 0.0139.

(I) Quantification showing unaffected secondary branch number per primary branch in control (black) versus EGFR-DN (gray). N = 17 primary branches, 4 individuals for control and EGFR-DN. Mann-Whitney test; ^{ns}p = 0.1462.

(J, K, L, P, and Q) (J) Quantification showing comparable BrpD3 mCherry puncta per unit branch length in control (black) versus EGFR-DN (gray). N = 59 primary branches, 10 individuals for control and N = 56 primary branches, 10 individuals for EGFR-DN. Mann-Whitney test; ^{ns}p = 0.36. EGFR activity blocked only late

(legend continued on next page)

Please cite this article in press as: Dutta et al., EGFR-dependent suppression of synaptic autophagy is required for neuronal circuit development, Current Biology (2022), https://doi.org/10.1016/j.cub.2022.12.039

medulla projecting neurons along with some lobula and lobula plate targeting neurons (Figures S3A1–S3A21). Their most frequent partners are lamina wide-field cells (Lawf1/2) (Figures S3A11, S3A18, and S3H), followed distantly by *trans* medulla neurons (Tm2/21/Y8/9) (Figures S3A2, S3A3, S3A7, S3A8, and S3H).[39] We further validated Lawf1 and Tm2 subtypes as DCN postsynaptic targets using activity-dependent GRASP (Figures S3C–S3D″). Next, we tested the effects of suppression of EGFR activity on DCN circuit wiring. We observed a drastic reduction in overall connectivity (Figures 3O–3Q, S2M, S2N, and S2P) in the medulla, with a significant reduction in the most frequent partners Lawf1/2, Tm2/21, and a complete loss of less frequent partners (Figure S3B). Therefore, the stabilization of AZs by EGFR is required for adult M-DCN connectivity.

We have shown that Brp knockdown causes an increase in secondary branches and that EGFR activity suppression results in a similar increase of secondary branches as well as a late loss of Brp puncta. We therefore asked whether a reduction of Brp might explain the secondary branching phenotype upon EGFR inactivation. To test this, we introduced an extra genomic copy of the *brp* gene in a DCN EGFR-DN background. Increasing Brp levels with one genomic copy rescued the loss of BrpD3-GFP puncta showing specificity of the phenotype (Figures 3R–3U). The secondary branching phenotype was also rescued (Figures 3R–3T and 3W), but not the primary branching phenotype associated with the early role of EGFR (Figures 3R–3T and 3V). Together these data show that EGFR inactivation causes loss of Brp, which in turn destabilizes terminal axon branches leading to an increase in their numbers. We conclude that Brp protein dosage and thereby number of AZs is a determinant of terminal branch stability.

Temporally specific requirement for EGFR activity in synapse formation and terminal branching dynamics

Early DCN branch pruning is regulated by EGFR via the control of actin dynamics, and EGFR is required during a second phase to maintain Brp and synaptic connectivity. Do these two effects reflect different temporal requirements of EGFR, or is the late EGFR-sensitive phenotype an indirect consequence of the early effect of EGFR on primary branching? To distinguish between these two possibilities, we temporally inactivated EGFR function at different times during development using the Gal4/Gal80 temperature-sensitive repressor system (Gal80^{ts}) combined with the EGFR-DN transgene and a GFP reporter of the Gal80^{ts} system (Figure 4). At 22°C (green bar), the Gal80^{ts} system is active and prevents GFP expression (Figure S3E) and thus EGFR-DN expression allowing EGFR activity. At 29°C (magenta bar) Gal80^{ts} is inactivated, allowing EGFR-DN to be expressed: EGFR activity will be inhibited. We additionally calibrated the temporal progression of branch development at 22°C with respect to control at 25°C (Figures S3F–S3J). As expected, continuous EGFR inactivation from P48 till adult resulted in a significant increase in primary and secondary branches and a significant decrease in Brp from adult branches (Figures 4A–4E). EGFR inactivation from P42 to P57 increases primary branches but has no effect on secondary branches or Brp (Figures 4F–4J). In contrast, inactivating EGFR from P55 (Figures 4K–4O) or P65 (Figures 4P–4T) has no effect on primary branch number but significantly increases secondary branches and significantly decreases Brp. EGFR role in synapse formation is strictly developmental as EGFR inactivation in adult did not cause branching or Brp levels and distribution defects (Figures S4A–S4E). Therefore, regulation of EGFR at presynaptic branches defines a developmental critical interval for terminal branch consolidation and synapse stabilization.

Suppression of EGFR function increases autophagosome formation and Brp localization to degradative compartments

Autophagy can regulate synapse formation by restricting filopodial kinetics[19] and EGFR has been shown to regulate autophagy in *Drosophila* testis[40] and tumorigenic contexts.[41] We hypothesized that EGFR activity may suppress autophagy in DCNs. Suppression of EGFR activity may therefore result in an upregulation of autophagy followed by an increased Brp degradation. To test this idea, we first used a membrane-associated degradation reporter (myr-mCherry-pHluorin). In fixed brains, this probe marks degradative compartments in red with little or no green fluorescent signal because mCherry is significantly more acidification- and degradation-resistant than the pHluorin.[42] In DCNs of control brains, we observed an mCherry/pHluorin intensity ratio of ~1, while EGFR inhibition led to a significant 2-fold increase of the mCherry/pHluorin ratio in large clusters (Figures S4F–S4H). This increased localization to degradative compartments was also observed with an mCherry-pHluorin-tagged version of the BrpD3 probe (Figures S4I–S4O). To understand the nature of these Brp-containing degradative compartments, we analyzed the colocalization of the BrpD3-GFP marker with endogenous Rab7 and a Rab7-RFP reporter at P65 and P72 and in adult brains. Upon EGFR inactivation, Rab7 was upregulated in adult cell bodies (Figures S5L–S5M′), and BrpD3-GFP colocalization with endogenous Rab7 in axon branches progressively

either from P55 (K–L″) or from P65 (P–Q″) throughout development leads to decreased BrpD3-mCherry puncta (K″, L″, P″, and Q″) and increased secondary branches (K′, L′, P′, and Q′) with no significant change in primary branches (K, L, P, and Q) in adult DCNs.

(M and R) Quantification showing unaffected primary branches per axon in control (black) versus EGFR-DN (gray). (M) n = 38 axons, N = 9 individuals for control and n = 43 axons, N = 10 individuals for EGFR-DN. Mann-Whitney test; ^{ns}p = 0538. (R) n = 36 axons, N = 7 individuals for control and n = 26 axons, N = 5 individuals for EGFR-DN. Mann-Whitney test; ^{ns}p = 7,204.

(N and S) Quantification showing increased secondary branches per primary branch in control (black) versus EGFR-DN (gray). (N) n = 22 primary branches, N = 4 individuals for control and n = 21 primary branches, N = 4 individuals for EGFR-DN. Mann-Whitney test; ****p < 0.0001. (S) n = 25 primary branches, N = 5 individuals for control; n = 26 primary branches, N = 5 individuals for EGFR-DN. Mann-Whitney test; ****p < 0.0001.

(O and T) Quantification showing decreased BrpD3-mCherry puncta per unit branch length in control (black) versus EGFR-DN (gray). (O) n = 47 primary branches, N = 7 individuals for control and n = 53 primary branches, N = 8 individuals for EGFR-DN. Mann-Whitney test; ****p < 0.0001. (T) N = 87 primary branches, 11 individuals for control and n = 94 primary branches, N = 12 individuals for EGFR-DN. Mann-Whitney test; ****p < 0.0001.

Error bars denote mean ± SEM; scale bar represents 5 μm.

See also Figures S3 and S4 and Data S1.

Please cite this article in press as: Dutta et al., EGFR-dependent suppression of synaptic autophagy is required for neuronal circuit development, Current Biology (2022), https://doi.org/10.1016/j.cub.2022.12.039

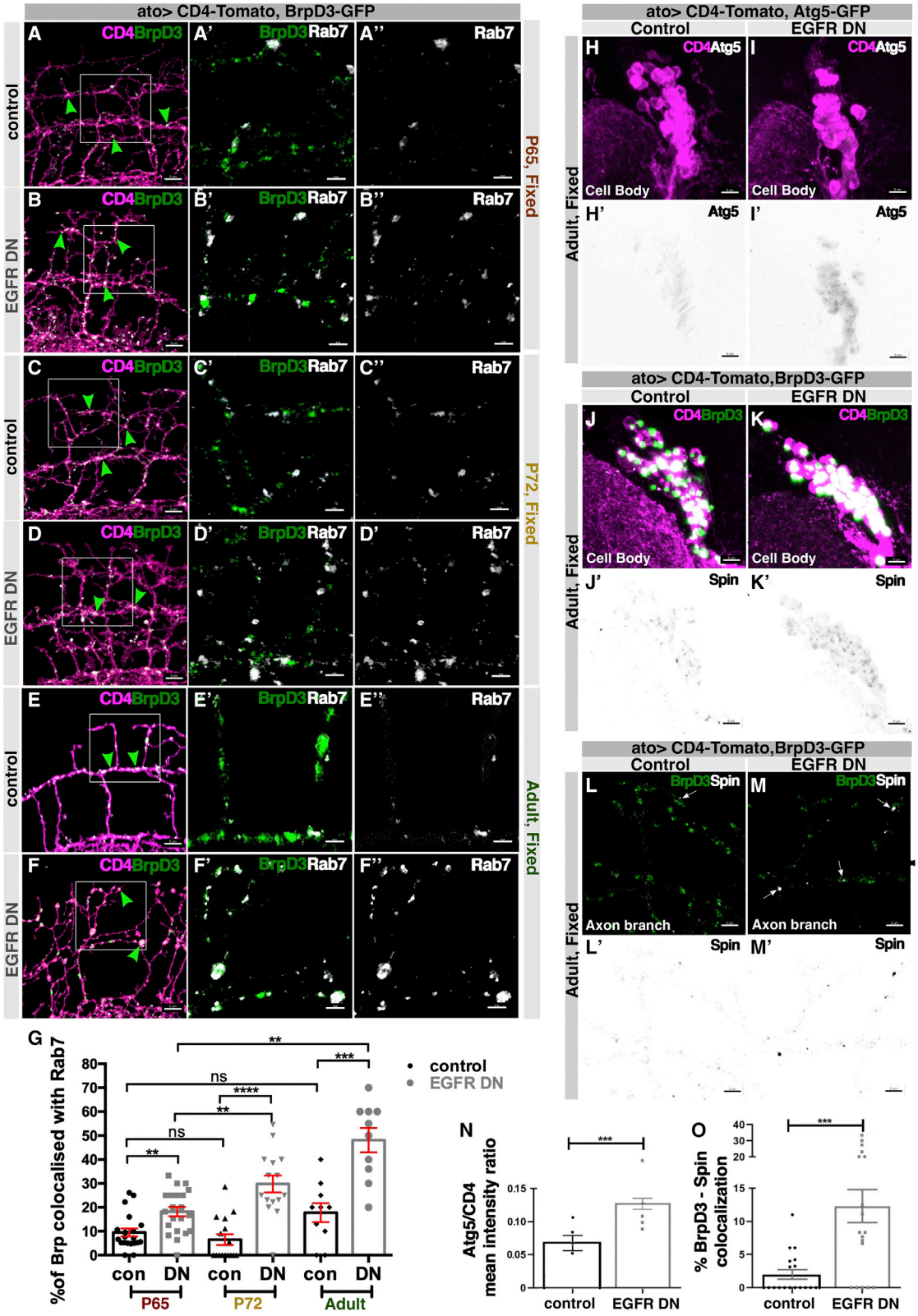

Figure 5. EGFR activity is required to prevent Brp degradation during synaptogenesis

(A–F) Progressively increased colocalization of endogenous Rab7 (white) with BrpD3-GFP puncta (green) in DCN axon terminals labeled with CD4-tomato (magenta) in control versus EGFR-DN during late development: P65 (A–B″), P72 (C–D″), and adult (E–F″). White squares represent regions of higher magnification showing Rab7-BrpD3 colocalization in (A)–(F″).

(legend continued on next page)

increased from P65 to adult (Figures 5A–5G). We obtained similar results using the Rab7-RFP reporter expressed specifically in DCNs (Figures S5A–S5D). In contrast, we did not observe any significant changes in Rab7-RFP colocalization with Syd1 puncta upon EGFR inactivation (Figures S5E–S5G). Thus, suppression of EGFR function leads to an increase of Rab7-positive Brp-containing degradative compartments.

The observed increase of degradative compartments could either result from a block of degradation or from increased levels of functional degradation. We therefore tested whether suppression of EGFR function leads to a selective accumulation of late degradative compartments (indicative of a block of degradation) or induces early markers of degradation. In addition to the Rab7 upregulation, we found upregulation of both early and late markers for autophagosomal degradation, including P62 (a cargo-adaptor for autophagic engulfment),[43] Atg5-GFP (an autophagosome formation marker),[44] endogenous Atg8 (a core protein of autophagosome maturation)[45,46] and endogenous Spinster (Spin), a lysosome and autolysosomes marker[47] (Figures 5H–5O, S5N–S5S, and S5W). Specifically, we observed upregulation of Atg5-GFP and p62 in discrete puncta specifically in DCN soma (Figures 5H, 5I, 5N, S5N, and S5O), whereas Atg8 and Spinster in both soma and axonal branches, where it colocalized with Brp (Figures 5J–5M, 5O, S5P–S5S, and S5W). Correspondingly, an Atg8-mCherry-pHluorin probe in DCNs of *ex vivo* cultured brains exhibited increased mCherry puncta volume (Figure S5V) with unaltered mCherry/GFP fluorescence ratio (Figure S5W) when EGFR was deactivated, indicating an increase of acidified, autophagosomal compartments (Figures S5T–S5W). This suggests that suppression of EGFR function leads to an activation of the entire autophagy pathway, starting with increased autophagosome formation.

EGFR suppression of autophagy maintains DCN presynaptic AZs and circuit connectivity

Our findings suggest that EGFR acts early in the autophagic cascade to protect synaptic material from degradation. If suppression of EGFR function leads to the induction of autophagosome formation and autophagic degradation, then blocking autophagy should prevent EGFR-dependent effects that are caused by autophagy upregulation. We therefore downregulated autophagic degradation through knockdown of *atg5*, *atg6*, or *rab7* in wild type and upon EGFR activity inhibition. We assayed terminal branching, BrpD3 distribution, and M-DCN postsynaptic connectivity. Knockdown of either atg5, atg6, or rab7 alone using well-characterized RNAi lines[48–50] did not cause significant changes in terminal secondary branch number or BrpD3 level (Figures 6A, 6A′, 6C, 6C′, 6M, 6N, S6A, S6C, and S6E). In contrast, knockdown of either *atg5*, *atg6*, or *rab7* upon EGFR inactivation all completely suppressed the increase in secondary branches and restored Brp at M-DCN synaptic terminals back to control levels (Figures 6D, 6D′, 6F, 6F′, 6M, 6N, S6B, S6D, and S6E), indicating that the synaptic loss caused by EGFR inactivation is autophagy dependent.

Our data suggest that EGFR is not required for increasing the levels of Brp import into the synaptic terminal, but instead for maintaining the Brp pool already present in presynaptic branches by preventing autophagic degradation. If Brp degradation is already fully suppressed by wild-type levels of EGFR activity, then increasing EGFR activity should not lead to an increase in Brp levels. We tested this idea by examining Brp upon expression of a constitutively activated EGFR (EGFR-CA)[51] in DCNs, which creates DCN over-branching defect.[29] We found no effect on BrpD3 density or distribution, DCN circuitry, nor on the degree of BrpD3 colocalization with Rab7-RFP (Figures S2M, S2O, S2P, and S5H–S5K).

Next, we asked whether the cell-autonomous rescue of presynaptic terminals suffices to restore M-DCN postsynaptic connectivity based on transsynaptic tracer experiments. Downregulation of either *atg6* or *rab7* alone resulted in an ~50% decrease in the number of *trans*-Tango-labeled M-DCN postsynaptic cells, while EGFR inactivation caused an almost complete loss of connectivity (Figures 6G–6J and 6O). However, knockdown of either *atg6* or *rab7* in EGFR-DN background rescued the connectivity to postsynaptic cells to the levels observed upon knockdown of *atg6* or *rab7* alone (Figures 6J–6L and 6O). Thus, the effect of EGFR inactivation on connectivity requires autophagy. Finally, we tested how these DCN connectivity changes caused by these manipulations affect behavior. We have previously shown that changes in M-DCN connectivity are sufficient to change behavioral responses in the multiparametric single fly visual response assay Buridan's paradigm.[28] In this assay, single flies walked freely between two identical visual cues (Figure S6F) and reduction of synapses increased fly activity when flies were tested at the same temperature at which they developed.[35] We first measured the baseline activity of individual flies in the absence of any DCN-relevant visual stimulus and observed that EGFR activity loss had no behavioral phenotype in the absence of a visual cue (Figures S6N–S6P). However, when subjected to stripes as visual stimuli, EGFR inactivation in DCNs results in behaviorally more active flies: longer walking distances, staying active for a longer time, and increasing the number of walks (Figures S6G, S6H, S6J, and S6K–S6M; Data S1). By contrast, *rab7* DCN-specific knockdown reduced behavioral

(G) Quantification showing increased percentage of BrpD3-GFP puncta colocalized with endogenous Rab7 per axon at P65, P72 and adults in control (black) versus $EGFR^{DN}$ (gray). n = 20 axons, N = 6 individuals for control versus n = 21 axons, N = 6 individuals for EGFR-DN at P65; n = 16 axons, N = 5 individuals for control versus n = 15 axons, N = 5individuals for EGFR-DN at P72, n = 10 axons, N = 5 individuals for control and EGFR-DN at adults. ****p < 0.0001, Kruskal-Wallis and Dunn's as post hoc test.

(H–M) Lack of EGFR activity results in increased and more puncta-like expression pattern of Atg5-GFP (I and I′) in the cell bodies of adult DCNs compared with control (H and H′), while Spinster shows similar increased expression pattern in the cell bodies (J–K′) and increased colocalization with BrpD3 puncta in the adult branches (L–M′).

(N) Quantification showing increased Atg5-GFP in adult DCN branches.

(O) Quantification showing increased colocalization of endogenous Spinster with BrpD3-GFP in the adult DCN branches. n = 19 axons, N = 6 individuals for control and EGFR-DN; ***p = 0.0005, Mann-Whitney test.

Scale bar represents 5 μm, apart from (A′)–(F″), which represents 3 μm.

See also Figures S4 and S5 and Data S1.

Please cite this article in press as: Dutta et al., EGFR-dependent suppression of synaptic autophagy is required for neuronal circuit development, Current Biology (2022), https://doi.org/10.1016/j.cub.2022.12.039

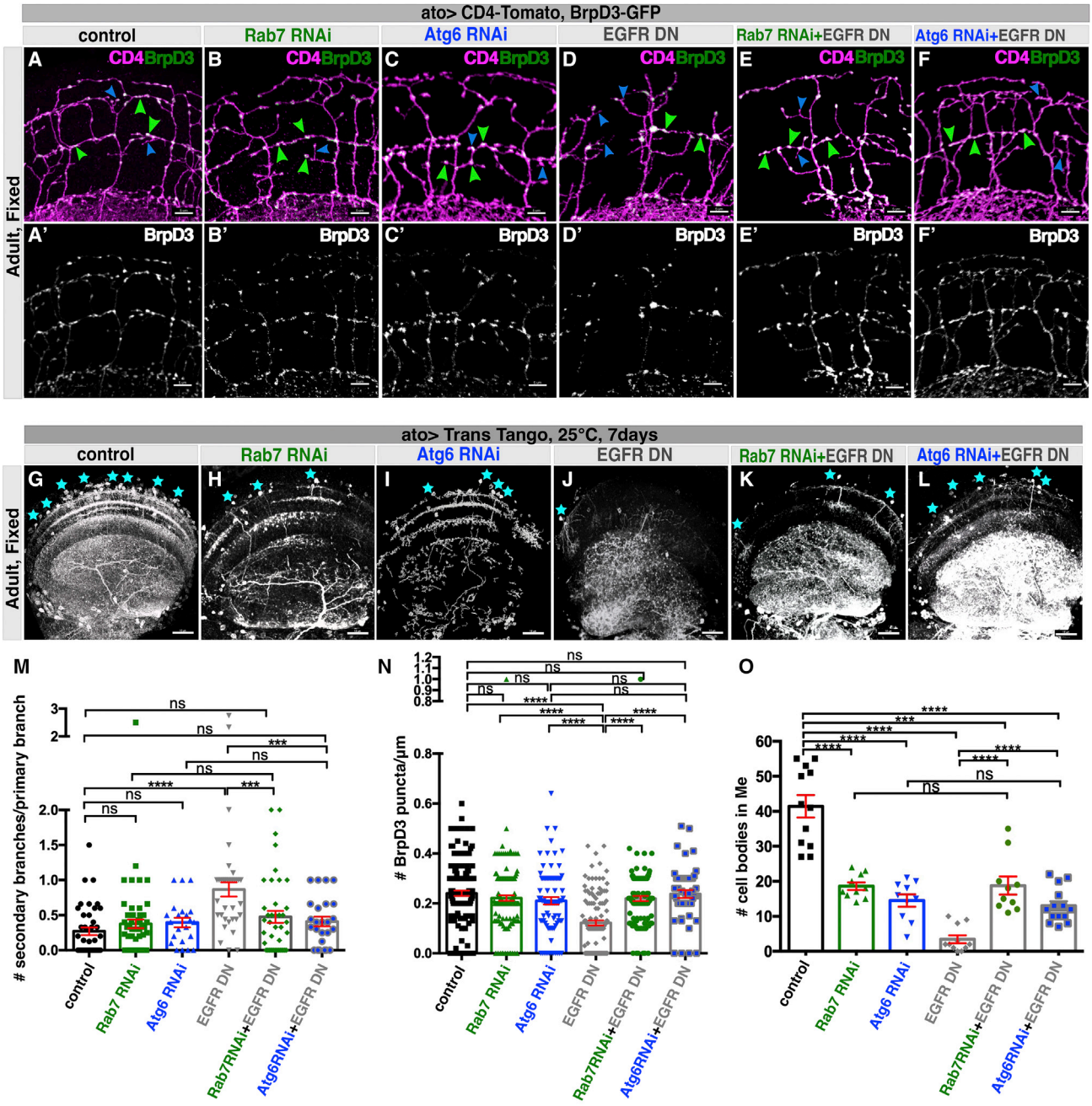

Figure 6. EGFR signals through autophagy to maintain DCN presynaptic active zone and circuit connectivity

(A–F) Rescuing loss of adult DCN terminal axon branch (magenta) number and BrpD3-GFP puncta (green) distribution in Rab7 RNAi + EGFR-DN (E and E′) and Atg6 RNAi + EGFR-DN (F and F′) back to the level of control (A and A′), Rab7-RNAi (B and B′), or Atg6-RNAi (C and C′) as compared with EGFR-DN (D and D′).

(G–L) Corresponding rescue of postsynaptic partner (cyan asterisks) loss in DCNs using *trans*-Tango at 25°C for 7-day-old adults in EGFR-DN (H) by expressing Rab7 RNAi + EGFR-DN (K) or Atg6 RNAi + EGFR-DN (L) back to the level of Rab7-RNAi (H) or Atg6-RNAi (I), respectively, but only partial rescue compared with control (G).

(M) Quantification showing rescue of secondary branch number per primary in Rab7 RNAi + EGFR-DN (green + gray) and Atg6 RNAi + EGFR-DN (blue + gray) back to the level of control (black), Rab7 RNAi (green), and Atg6 RNAi (blue) as compared with EGFR-DN (gray). n = 41 branches, N = 7 individuals for control; n = 50 branches, N = 8 individuals for Rab7 RNAi; n = 22 branches, N = 5 individuals for Atg6 RNAi; n = 35 branches, N = 6 individuals for EGFR-DN; n = 41 branches, N = 7 individuals for Rab7 RNAi + EGFR-DN; n = 25 branches, N = 5 individuals for Atg6 RNAi + EGFR-DN. Kruskal-Wallis and Dunn's as post hoc test; ****$p < 0.0001$.

(N) Quantification showing similar rescue of BrpD3-GFP puncta per unit branch length in Rab7 RNAi + EGFR-DN and Atg6 RNAi + EGFR-DN back to the level of control, Rab7 RNAi, and Atg6 RNAi as compared with EGFR-DN. n = 153 branches, N = 14 individuals for control; n = 138 branches, N = 10 individuals for Rab7

(legend continued on next page)

activity (Figures S6Q–S6S). Correspondingly, *rab7* knockdown in EGFR-DN background rescued the walking activity back to control levels (Figures S6H–S6M), suggesting that even partial rescue of DCN synaptic connectivity (Figure 6O) is sufficient to support normal locomotor activity at the level assayed here.

DISCUSSION

The complexity of neuronal circuit wiring patterns, driven to a significant extent by the degree of axonal branching during development,[6] is thought to be key to the emergence of behavior. In the mammalian motor cortex for example, axon branch complexity can allow a single neuron to innervate very distant ipsi- and contra-lateral cortical and sub-cortical targets.[52] The unique branching pattern of L-fibers supports the nocturnal lifestyle of the sweat bee *M. genalis*,[53] while intrinsic variation in M-DCN connectivity underlies individual variation in *Drosophila* visual response behavior.[28] Understanding the spatial, temporal, and mechanistic coordination of axonal branching and synaptogenesis during development is critical for a more complete description of the emergence of both conserved patterns and individual variation of neuronal circuit diagrams.

Here, we asked if, when, and how molecular factors that play key roles in regulating axon branching, synapse formation, and membrane degradation interact to produce specific presynaptic patterns, neuronal circuit connectivity and behavior using the developing *Drosophila* visual system as a model. This diverse list of cellular processes is tied together by their collaborative effects during the development of synaptic connectivity. Axo-dendritic branching and synapses formation have long been known to depend on each other during synaptotropic growth of branches based on synapse stabilization.[54] For example, branch stabilization during synaptotropic growth has also been shown to depend on synaptic activity and locally restricted calcium signals in developing *Drosophila* dendrites.[55] Developmental interactions of axonal and dendritic processes are a major contributor, and can sometimes predict, the adult synaptic connectivity.[7] By contrast, cell biological processes like cytoskeletal dynamics or membrane degradation have long been described as a "permissive" basis for more "instructive" molecular mechanisms of synaptic specification. However, to the extent that such cell biological mechanisms directly contribute to branching and synapse formation, they become parts of a composite instruction that cannot be pinned on a single molecular mechanism but require the consideration of several collaborating factors to understand a neuron's choice to branch and form a synapse.[56] Hence, an integrative analysis of molecular recognition, signaling, and cell biological machinery is necessary to mechanistically understand how branching contributes to adult synaptic connectivity.

Numerous molecular and cellular mechanisms have been implicated in the spatiotemporal control of how synaptic partners are brought together for synapse formation.[7] Over the last 25 years investigating the role of EGFR in nervous systems has demonstrated its roles in neural stem cell maintenance,[57] astrocyte and oligodendrocyte maturation,[58] axon regeneration,[59] and more recently in neurite outgrowth and branching.[60] In addition, we have recently demonstrated roles for the cell biological regulation of filopodial dynamics and autophagic degradation in establishing specific synaptic connectivity.[4,19] How such basic cellular processes are coupled to the process of patterning axonal branches and how the three processes—branching, synaptogenesis, and autophagy—are coordinated in time to establish circuit-specific wiring diagrams has remained unclear. We find that these processes are indeed coupled but only during a very specific temporal interval through EGFR activity preventing the autophagic degradation of the synaptic AZ protein Brp. Inactivation of EGFR during this specific critical interval in late development, but not before or after, causes Brp degradation, circuit wiring changes, and altered visually driven behaviors.

An interesting observation is the difference in dynamics upon EGFR inactivation and knockdown of Brp. While both result in increased secondary branches, loss of Brp leads to a more dynamic state of these branches even in the adult brain. In contrast, suppression of EGFR function causes these secondary branches to be largely static, even though EGFR inactivation also causes Brp loss. This is likely because suppression of EGFR function also impairs actin dynamics which are required for filopodial dynamics, while Brp loss does not affect EGFR activity and thus does not impair actin dynamics. These observations underline the critical importance of live imaging for discovering and interpreting otherwise seemingly similar phenotypes. These observations are also consistent with the genetic hierarchy we observed whereby EGFR regulates BrpD3 levels, but Brp does not appear to regulate EGFR levels. Again, live imaging combined with temporally restricted inactivation of EGFR allowed us to dissect the temporal logic of this genetic hierarchy and discover the role of EGFR activity as coupling mechanism between branching dynamics, local degradation, and synapse formation.

Our observations show that the coupling between branching, autophagy, and synaptogenesis is only required during a very specific temporal interval which, perhaps not surprisingly, coincides with active synaptogenesis in the developing fly brain.[61] Our analysis of the temporal sequence of trafficking of various molecules indicates that this developmental critical interval is opened by the spatial and temporal coincidence of EGFR and BrpD3 in exploratory branches. Similarly, it is likely that the critical interval ends once synaptic contacts between DCNs and their postsynaptic cells have been established. What remains to be explored is how exactly synapse formation ends the

RNAi; n = 84 branches, N = 9 individuals for Atg6 RNAi; n = 124 branches, N = 10 individuals for EGFR-DN; n = 122 branches, N = 10 individuals for Rab7 RNAi + EGFR-DN, n = 50 branches, N = 6 individuals for Atg6 RNAi + EGFR-DN; Kruskal-Wallis and Dunn's as post hoc test; ****$p < 0.0001$.

(O) Quantification for rescuing postsynaptic cell body number in medulla per optic lobe in Rab7 RNAi + EGFR-DN and Atg6 RNAi + EGFR-DN back to the level of control, Rab7 RNAi, and Atg6 RNAi as compared with EGFR-DN. n = 12 individual optic lobes in control, N = 11 individual optic lobes in Rab7 RNAi, N = 10 individual optic lobes in Atg6 RNAi, N = 13 individual optic lobes in EGFR-DN, N = 12 individual optic lobes in Rab7 RNAi + EGFR-DN, and N = 14 individual optic lobes in Atg6 RNAi + EGFR-DN. Kruskal-Wallis and Dunn's as post hoc test; ****$p < 0.0001$.

Error bars denote mean ± SEM; scale bar represents 5 μm, except for (G)–(L), where it is 15 μm.

See also Figure S6 and Data S1.

Please cite this article in press as: Dutta et al., EGFR-dependent suppression of synaptic autophagy is required for neuronal circuit development, Current Biology (2022), https://doi.org/10.1016/j.cub.2022.12.039

interactive feedback between branch dynamics and synapse degradation. One possibility is that postsynaptic dendrites provide molecular signals to presynaptic axonal branches to limit AZ degradation. Another possibility is that the initiation of spontaneous activity alters local endolysosomal recycling[62] to reduce degradation and favor maintenance, for example, through the activity-dependent regulation of local translation of resident mRNAs.[63] A third possibility is the late arrival of presynaptic proteins that protect the AZ, reduce autophagy, or alter EGFR function. Clearly, none of these mechanisms are mutually exclusive, and we speculate that a combination of such feedback mechanisms would be the best way to ensure a robust closing of the developmental critical interval we discovered here. Flies, similar to vertebrates, undergo a critical period of post-natal experience-dependent synaptic pruning with unknown molecular mechanism. It would be interesting to explore whether the mechanism we uncovered here also plays a role in synaptic regulation and neural circuit plasticity during that critical period. It is possible that similar molecular modules are used re-iteratively to regulate synaptic homeostasis and presynaptic branching in experience-independent and -dependent brain development.

We have previously shown that an increase in local autophagy also led to a decrease of adult synapses in R7 photoreceptor neurons,[19] albeit by a different mechanism. In R7 photoreceptors, local autophagosome formation at the tips of synaptogenic filopodia is accompanied by engulfment of synaptic seeding factors but not Brp, followed by filopodial collapse and thus less filopodial availability to form synapses. In DCNs, axonally localized autophagosome formation is accompanied by engulfment of Brp but not synaptic seeding factors, leading to a destabilization and reduction of mature synapses. Hence, the spatiotemporal-specific roles of autophagy in different types of axon terminals during synapse formation are highly context specific, involve different substrates, and yet lead to similar outcomes. An obvious contextual difference between R7s and DCNs is that only the latter form branched axons and employ synaptotropic-like branch stabilization through mature synapses.

Increasing evidence supports the important roles that stochastic and/or noisy molecular processes play in the early phases of establishing wiring specificity prior to the final step of spatially and temporally restricted local synapse formation and stabilization.[64] While neuronal circuit wiring patterns across the animal kingdom are highly robust, they, almost without exception, show at least some degree of intrinsic variation within and between individuals. Noise in genetically encoded program can ensure robustness of highly reproducible wiring patterns, for example, when stochastic exploration ensures partner finding.[65] Correspondingly, axon branch initiation in DCNs is noisy and exploratory, while the final axonal pattern is robustly stereotypic. The evidence presented in this work demonstrates the importance of intrinsic local control of the feedback between axonal branching and synapse formation to ensure the robust outcome. Such local feedback regulation ensures that genetically encoded noisy molecular and cellular processes such as filopodial growth and retraction and synaptic seeding are coordinated in time and space to produce conserved, robust, yet individually variable, non-random neuronal circuit diagrams.

STAR★METHODS

Detailed methods are provided in the online version of this paper and include the following:

- KEY RESOURCES TABLE
- RESOURCE AVAILABILITY
  - Lead contact
  - Materials availability
  - Data and code availability
- EXPERIMENTAL MODEL AND SUBJECT DETAILS
- METHOD DETAILS
  - Immunohistochemistry and fixed imaging
  - STED imaging
  - Pupal brain culture and Live-Imaging
  - Trans-tango and activity-dependent GRASP
  - Buridan's paradigm assay
- QUANTIFICATION AND STATISTICAL ANALYSIS
  - Branch number and length analysis
  - Synapse number analysis
  - Live tracing of molecules in branches
  - mCherry/pHluorin intensity and volume analysis
  - Colocalization analysis
  - Statistical analysis

SUPPLEMENTAL INFORMATION

Supplemental information can be found online at https://doi.org/10.1016/j.cub.2022.12.039.

ACKNOWLEDGMENTS

This work was supported by the Einstein-BIH program and DFG Research Unit 5289 RobustCircuit project P2 (to B.A.H. and P.R.H.), DFG Research Unit Syntophagy RP7 (Hi 1886/8), funding from the European Research Council (ERC) under the European Union's Horizon 2020 research and innovation programme (grant agreement no. 101019191 (to P.R.H.), the Investissements d'Avenir program (ANR-10-IAIHU-06), Paris Brain Institute-ICM core funding, the Paul G. Allen Frontiers Group Allen Distinguished Investigator grant, the Roger De Spoelberch Prize, and an NIH Brain Initiative RO1 grant (1R01NS121874-01) (to B.A.H.). M.A. is funded by the Fondation de la Recherche Medical (FRM) postdoctoral fellowship (ARF202005011913). We thank Dr. U. Habenicht from the Einstein Foundation Berlin for guidance throughout this project. We further thank the BioSupraMol Optical Microscopy facility for STED microscopy, members of the Hassan and Hiesinger labs for helpful discussions, and Drs. Stephan Sigrist and Dietmar Schmucker for comments on the manuscript.

AUTHOR CONTRIBUTIONS

S.B.D., B.A.H., and P.R.H. conceived the study and designed the experiments. S.B.D., G.A.L., and M.A. conducted all experiments and data analysis. S.B.D., M.A., G.A.L., B.A.H., and P.R.H. wrote the manuscript.

DECLARATION OF INTERESTS

The authors declare no competing interests.

INCLUSION AND DIVERSITY

One or more of the authors of this paper self-identifies as an underrepresented ethnic minority in their field of research and within their geographical location. We support inclusive, diverse, and equitable conduct of research.

Received: April 1, 2022
Revised: October 31, 2022
Accepted: December 14, 2022
Published: January 13, 2023

REFERENCES

1. Doll, C.A., and Broadie, K. (2014). Impaired activity-dependent neural circuit assembly and refinement in autism spectrum disorder genetic models. Front. Cell. Neurosci. *8*, 30.
2. Batool, S., Raza, H., Zaidi, J., Riaz, S., Hasan, S., and Syed, N.I. (2019). Synapse formation: from cellular and molecular mechanisms to neurodevelopmental and neurodegenerative disorders. J. Neurophysiol. *121*, 1381–1397.
3. del Pino, I., Rico, B., and Marín, O. (2018). Neural circuit dysfunction in mouse models of neurodevelopmental disorders. Curr. Opin. Neurobiol. *48*, 174–182.
4. Özel, M.N., Kulkarni, A., Hasan, A., Brummer, J., Moldenhauer, M., Daumann, I.M., Wolfenberg, H., Dercksen, V.J., Kiral, F.R., Weiser, M., et al. (2019). Serial synapse formation through filopodial competition for synaptic seeding factors. Dev. Cell *50*, 447–461.e8.
5. Bodakuntla, S., Nedozralova, H., Basnet, N., and Mizuno, N. (2021). Cytoskeleton and membrane organization at axon branches. Front. Cell Dev. Biol. *9*, 707486.
6. Hoersting, A.K., and Schmucker, D. (2021). Axonal branch patterning and neuronal shape diversity: roles in developmental circuit assembly: axonal branch patterning and neuronal shape diversity in developmental circuit assembly. Curr. Opin. Neurobiol. *66*, 158–165.
7. Agi, E., Kulkarni, A., and Hiesinger, P.R. (2020). Neuronal strategies for meeting the right partner during brain wiring. Curr. Opin. Neurobiol. *63*, 1–8.
8. Chia, P.H., Chen, B., Li, P., Rosen, M.K., and Shen, K. (2014). Local F-actin network links synapse formation and axon branching. Cell *156*, 208–220.
9. Meyer, M.P., and Smith, S.J. (2006). Evidence from in vivo imaging that synaptogenesis guides the growth and branching of axonal arbors by two distinct mechanisms. J. Neurosci. *26*, 3604–3614.
10. Ruthazer, E.S., Li, J., and Cline, H.T. (2006). Stabilization of axon branch dynamics by synaptic maturation. J. Neurosci. *26*, 3594–3603.
11. Niell, C.M. (2006). Theoretical analysis of a synaptotropic dendrite growth mechanism. J. Theor. Biol. *241*, 39–48.
12. Bourgeois, J.P., and Rakic, P. (1993). Changes of synaptic density in the primary visual cortex of the macaque monkey from fetal to adult stage. J. Neurosci. *13*, 2801–2820.
13. Hua, J.Y., and Smith, S.J. (2004). Neural activity and the dynamics of central nervous system development. Nat. Neurosci. *7*, 327–332.
14. Cisneros-Franco, J.M., Voss, P., Thomas, M.E., and de Villers-Sidani, E. (2020). Critical periods of brain development. Handb. Clin. Neurol. *173*, 75–88.
15. Feller, M.B., and Scanziani, M. (2005). A precritical period for plasticity in visual cortex. Curr. Opin. Neurobiol. *15*, 94–100.
16. Fleming, A., and Rubinsztein, D.C. (2020). Autophagy in neuronal development and plasticity. Trends Neurosci. *43*, 767–779.
17. Xiong, W., Wei, W., Qi, Y., Du, Z., Qu, T., Liu, K., and Gong, S. (2020). Autophagy is required for remodeling in postnatal developing ribbon synapses of cochlear inner hair cells. Neuroscience *431*, 1–16.
18. Bhukel, A., Beuschel, C.B., Maglione, M., Lehmann, M., Juhász, G., Madeo, F., and Sigrist, S.J. (2019). Autophagy within the mushroom body protects from synapse aging in a non-cell autonomous manner. Nat. Commun. *10*, 1318.
19. Kiral, F.R., Linneweber, G.A., Mathejczyk, T., Georgiev, S.V., Wernet, M.F., Hassan, B.A., von Kleist, M., and Hiesinger, P.R. (2020). Autophagy-dependent filopodial kinetics restrict synaptic partner choice during Drosophila brain wiring. Nat. Commun. *11*, 1325.
20. Shen, W., and Ganetzky, B. (2009). Autophagy promotes synapse development in Drosophila. J. Cell Biol. *187*, 71–79.
21. Tang, G., Gudsnuk, K., Kuo, S.H., Cotrina, M.L., Rosoklija, G., Sosunov, A., Sonders, M.S., Kanter, E., Castagna, C., Yamamoto, A., et al. (2014). Loss of mTOR-dependent macroautophagy causes autistic-like synaptic pruning deficits. Neuron *83*, 1131–1143.
22. Azarnia Tehran, D., Kuijpers, M., and Haucke, V. (2018). Presynaptic endocytic factors in autophagy and neurodegeneration. Curr. Opin. Neurobiol. *48*, 153–159.
23. Wang, M.M., Feng, Y.S., Yang, S.D., Xing, Y., Zhang, J., Dong, F., and Zhang, F. (2019). The relationship between autophagy and brain plasticity in neurological diseases. Front. Cell. Neurosci. *13*, 228.
24. Adnan, G., Rubikaite, A., Khan, M., Reber, M., Suetterlin, P., Hindges, R., and Drescher, U. (2020). The GTPase Arl8B plays a principle role in the positioning of interstitial axon branches by spatially controlling autophagosome and lysosome location. J. Neurosci. *40*, 8103–8118.
25. Hassan, B.A., Bermingham, N.A., He, Y., Sun, Y., Jan, Y.N., Zoghbi, H.Y., and Bellen, H.J. (2000). Atonal regulates neurite arborization but does not act as a proneural gene in the Drosophila brain. Neuron *25*, 549–561.
26. Langen, M., Koch, M., Yan, J., De Geest, N., Erfurth, M.L., Pfeiffer, B.D., Schmucker, D., Moreau, Y., and Hassan, B.A. (2013). Mutual inhibition among postmitotic neurons regulates robustness of brain wiring in Drosophila. eLife *2*, e00337.
27. Srahna, M., Leyssen, M., Choi, C.M., Fradkin, L.G., Noordermeer, J.N., and Hassan, B.A. (2006). A signaling network for patterning of neuronal connectivity in the Drosophila brain. PLoS Biol. *4*, e348.
28. Linneweber, G.A., Andriatsilavo, M., Dutta, S.B., Bengochea, M., Hellbruegge, L., Liu, G., Ejsmont, R.K., Straw, A.D., Wernet, M., Hiesinger, P.R., et al. (2020). A neurodevelopmental origin of behavioral individuality in the Drosophila visual system. Science *367*, 1112–1119.
29. Zschätzsch, M., Oliva, C., Langen, M., De Geest, N., Özel, M.N., Williamson, W.R., Lemon, W.C., Soldano, A., Munck, S., Hiesinger, P.R., et al. (2014). Regulation of branching dynamics by axon-intrinsic asymmetries in tyrosine kinase receptor signaling. eLife *3*, e01699.
30. Fouquet, W., Owald, D., Wichmann, C., Mertel, S., Depner, H., Dyba, M., Hallermann, S., Kittel, R.J., Eimer, S., and Sigrist, S.J. (2009). Maturation of active zone assembly by Drosophila Bruchpilot. J. Cell Biol. *186*, 129–145.
31. Owald, D., Fouquet, W., Schmidt, M., Wichmann, C., Mertel, S., Depner, H., Christiansen, F., Zube, C., Quentin, C., Körner, J., et al. (2010). A Syd-1 homologue regulates pre- and postsynaptic maturation in Drosophila. J. Cell Biol. *188*, 565–579.
32. Buff, E., Carmena, A., Gisselbrecht, S., Jiménez, F., and Michelson, A.M. (1998). Signalling by the Drosophila epidermal growth factor receptor is required for the specification and diversification of embryonic muscle progenitors. Development *125*, 2075–2086.
33. Wagh, D.A., Rasse, T.M., Asan, E., Hofbauer, A., Schwenkert, I., Dürrbeck, H., Buchner, S., Dabauvalle, M.C., Schmidt, M., Qin, G., et al. (2006). Bruchpilot, a protein with homology to ELKS/CAST, is required for structural integrity and function of synaptic active zones in Drosophila. Neuron *49*, 833–844.
34. Spinner, M.A., Walla, D.A., and Herman, T.G. (2018). Drosophila syd-1 has rhogap activity that is required for presynaptic clustering of bruchpilot/elks but not neurexin-1. Genetics *208*, 705–716.
35. Kiral, F.R., Dutta, S.B., Linneweber, G.A., Hilgert, S., Poppa, C., Duch, C., von Kleist, M., Hassan, B.A., and Hiesinger, P.R. (2021). Brain connectivity inversely scales with developmental temperature in Drosophila. Cell Rep. *37*, 110145.
36. Huang, S., Piao, C., Beuschel, C.B., Götz, T., and Sigrist, S.J. (2020). Presynaptic active zone plasticity encodes sleep need in Drosophila. Curr. Biol. *30*, 1077–1091.e5.
37. Fulterer, A., Andlauer, T.F.M., Ender, A., Maglione, M., Eyring, K., Woitkuhn, J., Lehmann, M., Matkovic-Rachid, T., Geiger, J.R.P., Walter, A.M., et al. (2018). Active zone scaffold protein ratios tune functional diversity across brain synapses. Cell Rep. *23*, 1259–1274.

38. Talay, M., Richman, E.B., Snell, N.J., Hartmann, G.G., Fisher, J.D., Sorkaç, A., Santoyo, J.F., Chou-Freed, C., Nair, N., Johnson, M., et al. (2017). Transsynaptic mapping of second-order taste neurons in flies by trans-tango. Neuron *96*, 783–795.e4.

39. Fischbach, K.-F., and Dittrich, A.P.M. (1989). The optic lobe of Drosophila melanogaster. I. A Golgi analysis of wild-type structure. Cell Tissue Res. *258*.

40. Sênos Demarco, R., and Jones, D.L. (2020). EGFR signaling promotes basal autophagy for lipid homeostasis and somatic stem cell maintenance in the Drosophila testis. Autophagy *16*, 1145–1147.

41. Wu, M., and Zhang, P. (2020). EGFR-mediated autophagy in tumourigenesis and therapeutic resistance. Cancer Lett. *469*, 207–216.

42. Jin, E.J., Kiral, F.R., Ozel, M.N., Burchardt, L.S., Osterland, M., Epstein, D., Wolfenberg, H., Prohaska, S., and Hiesinger, P.R. (2018). Live observation of two parallel membrane degradation pathways at axon terminals. Curr. Biol. *28*, 1027–1038.e4.

43. Nezis, I.P., Simonsen, A., Sagona, A.P., Finley, K., Gaumer, S., Contamine, D., Rusten, T.E., Stenmark, H., and Brech, A. (2008). Ref(2)P, the Drosophila melanogaster homologue of mammalian p62, is required for the formation of protein aggregates in adult brain. J. Cell Biol. *180*, 1065–1071.

44. Juhász, G., Hill, J.H., Yan, Y., Sass, M., Baehrecke, E.H., Backer, J.M., and Neufeld, T.P. (2008). The class III PI(3)K Vps34 promotes autophagy and endocytosis but not TOR signaling in Drosophila. J. Cell Biol. *181*, 655–666.

45. Martens, S., and Fracchiolla, D. (2020). Activation and targeting of ATG8 protein lipidation. Cell Discov. *6*, 23.

46. Wirth, M., Zhang, W., Razi, M., Nyoni, L., Joshi, D., O'Reilly, N., Johansen, T., Tooze, S.A., and Mouilleron, S. (2019). Molecular determinants regulating selective binding of autophagy adapters and receptors to ATG8 proteins. Nat. Commun. *10*, 2055.

47. Rong, Y., McPhee, C.K., Deng, S., Huang, L., Chen, L., Liu, M., Tracy, K., Baehrecke, E.H., Yu, L., and Lenardo, M.J. (2011). Spinster is required for autophagic lysosome reformation and mTOR reactivation following starvation. Proc. Natl. Acad. Sci. USA *108*, 7826–7831.

48. Lőrincz, P., Lakatos, Z., Varga, Á., Maruzs, T., Simon-Vecsei, Z., Darula, Z., Benkő, P., Csordás, G., Lippai, M., Andó, I., et al. (2016). MiniCORVET is a Vps8-containing early endosomal tether in Drosophila. eLife *5*, e14226.

49. Manent, J., Banerjee, S., De Matos Simoes, R., Zoranovic, T., Mitsiades, C., Penninger, J.M., Simpson, K.J., Humbert, P.O., and Richardson, H.E. (2017). Autophagy suppresses Ras-driven epithelial tumourigenesis by limiting the accumulation of reactive oxygen species. Oncogene *36*, 5576–5592.

50. Billes, V., Kovács, T., Manzéger, A., Lőrincz, P., Szincsák, S., Regős, Á., Kulcsár, P.I., Korcsmáros, T., Lukácsovich, T., Hoffmann, G., et al. (2018). Developmentally regulated autophagy is required for eye formation in Drosophila. Autophagy *14*, 1499–1519.

51. Queenan, A.M., Ghabrial, A., and Schüpbach, T. (1997). Ectopic activation of torpedo/egfr, a Drosophila receptor tyrosine kinase,dorsalizes both the eggshell and the embryo. Development *124*, 3871–3880.

52. Economo, M.N., Clack, N.G., Lavis, L.D., Gerfen, C.R., Svoboda, K., Myers, E.W., and Chandrashekar, J. (2016). A platform for brain-wide imaging and reconstruction of individual neurons. eLife *5*, e10566.

53. Grueber, W.B., Yang, C.H., Ye, B., and Jan, Y.N. (2005). The development of neuronal morphology in insects. Curr. Biol. *15*, R730–R738.

54. Vaughn, J.E., Barber, R.P., and Sims, T.J. (1988). Dendritic development and preferential growth into synaptogenic fields: a quantitative study of Golgi-impregnated spinal motor neurons. Synapse *2*, 69–78.

55. Ryglewski, S., Vonhoff, F., Scheckel, K., and Duch, C. (2017). Intraneuronal competition for synaptic partners conserves the amount of dendritic building material. Neuron *93*, 632–645.e6.

56. Hiesinger, P.R. (2021). Brain wiring with composite instructions. BioEssays *43*, e2000166.

57. Aguirre, A., Rubio, M.E., and Gallo, V. (2010). Notch and EGFR pathway interaction regulates neural stem cell number and self-renewal. Nature *467*, 323–327.

58. Galvez-Contreras, A.Y., Quiñones-Hinojosa, A., and Gonzalez-Perez, O. (2013). The role of EGFR and ErbB family related proteins in the oligodendrocyte specification in germinal niches of the adult mammalian brain. Front. Cell. Neurosci. *7*, 258.

59. Koprivica, V., Cho, K.S., Park, J.B., Yiu, G., Atwal, J., Gore, B., Kim, J.A., Lin, E., Tessier-Lavigne, M., Chen, D.F., et al. (2005). EGFR activation mediates inhibition of axon regeneration by myelin and chondroitin sulfate proteoglycans. Science *310*, 106–110.

60. Goldshmit, Y., Walters, C.E., Scott, H.J., Greenhalgh, C.J., and Turnley, A.M. (2004). SOCS2 induces neurite outgrowth by regulation of epidermal growth factor receptor activation. J. Biol. Chem. *279*, 16349–16355.

61. Fröhlich, A., and Meinertzhagen, I.A. (1982). Synaptogenesis in the first optic neuropile of the fly's visual system. J. Neurocytol. *11*, 159–180.

62. Tagliatti, E., Fadda, M., Falace, A., Benfenati, F., and Fassio, A. (2016). Arf6 regulates the cycling and the readily releasable pool of synaptic vesicles at hippocampal synapse. eLife *5*, e10116.

63. Rajgor, D., Welle, T.M., and Smith, K.R. (2021). The coordination of local translation, membranous organelle trafficking, and synaptic plasticity in neurons. Front. Cell Dev. Biol. *9*, 711446.

64. Hassan, B.A., and Hiesinger, P.R. (2015). Beyond molecular codes: simple rules to wire complex brains. Cell *163*, 285–291.

65. Hiesinger, P.R., and Hassan, B.A. (2018). The evolution of variability and robustness in neural development. Trends Neurosci. *41*, 577–586.

66. Schmid, A., Hallermann, S., Kittel, R.J., Khorramshahi, O., Frölich, A.M., Quentin, C., Rasse, T.M., Mertel, S., Heckmann, M., and Sigrist, S.J. (2008). Activity-dependent site-specific changes of glutamate receptor composition in vivo. Nat. Neurosci. *11*, 659–666.

67. Konstantinides, N. (2018). Phenotypic convergence: distinct transcription factors regulate common terminal features. Cell *174*, 622–635.e13.

68. Ting, C.Y., Gu, S., Guttikonda, S., Lin, T.Y., White, B.H., and Lee, C.H. (2011). Focusing transgene expression in Drosophila by coupling Gal4 with a novel split-Lex A expression system. Genetics *188*, 229–233.

69. Pooryasin, A., Maglione, M., Schubert, M., Matkovic-Rachid, T., Hasheminasab, S.M., Pech, U., Fiala, A., Mielke, T., and Sigrist, S.J. (2021). Unc13A and Unc13B contribute to the decoding of distinct sensory information in Drosophila. Nat. Commun. *12*, 1932.

70. Özel, M.N., Langen, M., Hassan, B.A., and Hiesinger, P.R. (2015). Filopodial dynamics and growth cone stabilization in Drosophila visual circuit development. eLife *4*, e10721.

Please cite this article in press as: Dutta et al., EGFR-dependent suppression of synaptic autophagy is required for neuronal circuit development, Current Biology (2022), https://doi.org/10.1016/j.cub.2022.12.039

STAR★METHODS

KEY RESOURCES TABLE

REAGENT or RESOURCE	SOURCE	IDENTIFIER
Antibodies		
Mouse anti-NC82 [1:10]	DSHB	AB 2314866
Mouse anti-GFP mAb [1:500]	Life Technologies	Cat# A11120; RRID: AB_221568
Chicken anti-GFP pAb [1:250]	Abcam	Cat# AB13970; RRID: AB_300798
Goat anti-GFP [1:500}	Abcam	Cat# AB6678
Rabbit anti-CD4 [1:250}	Atlas Antibodies	Cat# HPA004252; RRID: AB_1078466
Rabbit anti-dsRed [1:200}	Takara Bio	Cat# 632496; RRID: AB_10013483
Mouse anti-LacZ [1:200]	Promega	Cat# Z3781; RRID: AB_430877
Goat anti-mCherry [1:500]	Sicgen	Cat# AB 0040-200; RRID: AB_2333093
Rabbit anti-Rab7 mAb [1:1000]	Gift from Patrick Dolph	N/A
Rabbit anti-p62 [1:1000]	Gift from Gabor Juhasz	N/A
Guinea-pig anti-Spinster [1:1000]	Gift from Sean Sweeney	N/A
Guinea-pig anti-Unc13a [1:300]	Gift from Stephan Sigrist	N/A
Rabbit anti- GABARAP+GABARAPL1+GABARAPL2 (ATG8)	Abcam	Cat# AB109364; RRID: AB_10861928
STAR RED-coupled goat anti-chicken [1:250]	Abberior dyes	N/A
Donkey anti-chicken Alexa Fluor 488 [1:500]	Jackson ImmunoResearch Labs	Cat# 703.545.155; RRID: AB_2336933
Donkey anti-chicken Cy3 [1:500]	Jackson ImmunoResearch Labs	Cat# 703-545-155; RRID: AB_2340415
Donkey anti-mouse 488 [1:500]	Jackson ImmunoResearch Labs	Cat# 715-545-150; RRID: AB_2340846
Goat anti-guinea pig Alexa Flour 647 [1:500]	Jackson ImmunoResearch Labs	Cat# 106-605-003; RRID: AB_2337446
Donkey anti-rabbit Alexa Cy3 [1:500]	Jackson ImmunoResearch Labs	Cat# 711-165-152; RRID: AB_2307443
Donkey anti-mouse Alexa 405 [1:500]	Jackson ImmunoResearch Labs	Cat# 715.475.150; RRID: AB_2340758
Donkey anti-goat Alexa 647 [1:500]	Jackson ImmunoResearch Labs	Cat# 705-605-147; RRID: AB_2340437
Donkey anti-rabbit Alexa 647 [1:500]	Jackson ImmunoResearch Labs	Cat# 11-605-152; RRID: AB_2492288
Donkey anti-mouse Alexa 594 [1:500]	ThermoFisher Scientific	Cat# R37115; RRID: AB_2556543
Goat Anti-rabbit Alexa488 [1:100]	Thermofischer Scientific	Cat# A-11008; RRID: AB_143165
Goat Anti-mouse Alexa594 [1:100]	Thermofischer Scientific	Cat# A-11012; RRID: AB_2534079
Chemicals, peptides, and recombinant proteins		
Vectashield	Vector Laboratories	H-1000
PBS	GIBCO	70011-36
Prolong Gold	ThermoFisher Scientific	Cat# P10144
Formaldehyde	Merck KGaA	1.03999.1000
Triton X-100	Sigma-Aldrich	T8787
Schneider's *Drosophila* Medium [+] L-Glutamine	GIBCO	21720-024
Agarose, low gelling temperature	Sigma-Aldrich	A9045-10G
Human insulin recombinant zinc	GIBCO	12585014
Penicillin/Streptomycin	GIBCO	15140122
ES Cell FBS	GIBCO	16141-061
60 x 15mm culture plate	CytoOne	CC7672-3359
Sylgard 184	Dow Corning	N/A
Sodium Azide	Sigma	N/A
SilGard and Silicone Elastomer Kit	Dow Corning	184
Normal Donkey Serum	Jackson Immunoresearch	Cat# 017-000-121
Experimental models: Organisms/strains		
Drosophila: UAS-BrpD3::GFP	Gift from S.Sigrist[66]	N/A
Drosophila: UAS-BrpD3-mCherryPhlourin	Gift from R.Hiesinger	N/A

(*Continued on next page*)

Please cite this article in press as: Dutta et al., EGFR-dependent suppression of synaptic autophagy is required for neuronal circuit development, Current Biology (2022), https://doi.org/10.1016/j.cub.2022.12.039

Continued

REAGENT or RESOURCE	SOURCE	IDENTIFIER
Drosophila: UAS-myr-mCherrypHlourin	Gift from R.Hiesinger[42]	N/A
Drosophila: trans-Tango	Bloomington Drosophila Stock Center	RRID: BDSC_77123
Drosophila: M-DCN-Gal4	Vienna Drosophila Stock Center	RRID: VT037804_VDRC
Drosophila: UAS-LacZ	Bloomington Drosophila Stock Center	RRID: BDSC_3956
Drosophila: UAS-EGFR CA	Hassan lab[29]	N/A
Drosophila: UAS-EGFR GFP	Hassan lab[29]	N/A
Drosophila: UAS-Brp B3.C8 RNAi	Gift from S.Sigrist	N/A
Drosophila: Lawf1-Gal4	Gift from M.Reiser[67]	N/A
Drosophila: Tm2-Gal4	Ting et al.[68]	N/A
Drosophila: ato-Gal4-14a	Hassan lab[25]	N/A
Drosophila: ato-LexA	Hassan lab[26]	N/A
Drosophila: UAS-Trans Tango[38]	Bloomington Drosophila Stock Center	RRID: BDSC_77124
Drosophila: UAS-nSyb-spGFP1-10,lexAop-CD4-spGFP	Bloomington Drosophila Stock Center	RRID: BDSC_64314
Drosophila: lexAop-nSyb-spGFP1-10,UAS-CD4-spGFP11	Bloomington Drosophila Stock Center	RRID: BDSC_64315
Drosophila: UAS-Rab7 RFP	Gift from R.Hiesinger	N/A
Drosophila: UAS-EGFR DN	Gift from R. Hiesinger	N/A
Drosophila: UAS-Syd1 GFP	Gift from S.Sigrist	N/A
Drosophila: UAS-Brp B3.C8 RNAi	Gift from S.Sigrist[33]	FlyBase: FBal0195570; FlyBase: FBal0195571
Drosophila: UAS-BrpD3 mCherry	Gift from S. Sigrist[66]	N/A
Drosophila: UAS-mCD8::tdGFP	Bloomington Drosophila Stock Center	RRID: BDSC_5137
Drosophila: UAS-mCD4::tdGFP	Bloomington Drosophila Stock Center	RRID: BDSC_35836
Drosophila: UAS-mCD4::tdTomato	Bloomington Drosophila Stock Center	RRID: BDSC_35837
Drosophila: UAS-Rab7 RNAi	Vienna Drosophila Stock Center	VDRC 40337
Drosophila: UAS-Atg5 RNAi	Vienna Drosophila Stock Center	VDRC 104461
Drosophila: UAS-Syd1 RNAi	Bloomington Drosophila Stock Center	RRID: BDSC 32946
Drosophila: UAS-Atg6 RNAi	Vienna Drosophila Stock Center	VDRC GD 22122
Drosophila: UAS-EGFR CA	gift from T. Lecuit[29]	N/A
Drosophila: UAS-tubulin Gal80ts	Bloomington Drosophila Stock Center	RRID: BDSC 7017
Drosophila: UAS-Atg8-mCherry-GFP	Bloomington Drosophila Stock Center	RRID: BDSC_37749
Drosophila: Pacman Brp	Gift from S. Sigrist[36]	N/A
Drosophila: w1118	Bloomington Drosophila Stock Center	RRID: BDSC_54608
Drosophila: valium 20	Bloomington Drosophila Stock Center	N/A
Drosophila: valium 10	Bloomington Drosophila Stock Center	RRID: BDSC_35788
Drosophila: Canton-S	Bloomington Drosophila Stock Center	RRID: BDSC_
Drosophila: UAS-Wasp RNAi	Vienna Drosophila Stock Center	VDRC 108220
Drosophila: UAS-Ensconsin RNAi	Vienna Drosophila Stock Center	VDRC 106270
Drosophila: UAS-Act42a RNAi	Vienna Drosophila Stock Center	VDRC 12456
Drosophila: Canton S	Bloomington Drosophila Stock Center	N/A
Software and algorithms		
GraphPad Prism	GraphPad Software	RRID: SCR_002798
ImageJ	National Institutes of Health (NIH)	RRID: SCR_002285
IMARIS	Bitplane AG	RRID: SCR_007370
Leica Application Suite X	Leica Microsystems	RRID: SCR_013673
Clampfit	Axon Instruments	RRID: SCR_011323
Clampex	Axon Instruments	RRID: SCR_011323

Please cite this article in press as: Dutta et al., EGFR-dependent suppression of synaptic autophagy is required for neuronal circuit development, Current Biology (2022), https://doi.org/10.1016/j.cub.2022.12.039

RESOURCE AVAILABILITY

Lead contact

Further information and requests for resources and reagents should be directed to and will be fulfilled by the lead contact, Bassem Hassan (bassem.hassan@icm-institute.org).

Materials availability

This study did not generate new unique reagents.

Data and code availability

- This paper does not report original code.
- This paper does not report single cell RNAseq data and no western blots were performed. Microscopy data reported will be shared by the lead contact upon request.
- Any additional information required to reanalyze the data reported in this paper is available from the lead contact upon request.

EXPERIMENTAL MODEL AND SUBJECT DETAILS

Flies were reared at 25°C on standard cornmeal/yeast diet for all crosses and at 21°C and 29°C for Gal80ts experiments. For developmental analyses, white pre-pupae (P+0%) were collected and incubated at 25°C to pupal stages as stated on figures. See the key resources table for the detail of *Drosophila* strains.

METHOD DETAILS

Immunohistochemistry and fixed imaging

Pupal and adult brains were dissected in cold Schneider's Drosophila medium and fixed in 4% paraformaldehyde (PFA) in PBS for ~20 minutes. Tissues were then washed in PBST (1% Triton-X) on a shaker for 3x15mins followed by overnight incubation with primary antibodies at 4°C shaker. See the key resources table for the list and concentration of primary and secondary antibodies used in this study. Next, the brains were washed again with 1% PBST on a shaker for 3x15mins. The brains were incubated with appropriate secondary antibodies (Alexa 488, 554, 647, 405, 594) at a concentration of 1:500 from Jackson Immunoresearch Laboratories for 5-6hours at room temperature, followed by final wash with 1% PBST for 3x15mins. Tissues were mounted on taped cover slides using vector shield. Images were obtained with a Leica TCS SP8-X white laser confocal microscope with a 63x glycerol objective (NA=1.3) following the procedure from Kiral et al.[35] and Jin et al.[42]

STED imaging

Adult brains were dissected in cold Schneider's Drosophila medium and fixed in 4% paraformaldehyde (PFA) in PBS for ~20 minutes. Tissues were then in PBST (1% Triton-X) on a shaker for 3x15mins followed by overnight incubation with primary antibodies at 4°C shaker. See the key resources table for the list and concentration of primary and secondary antibodies used in this study. Next, the brains were washed again with 1% PBST on a shaker for 3x15mins. The brains were incubated in secondary antibodies for 5-6hours, followed by final wash with 1% PBST for 3x15mins. Then they were mounted on taped cover slides using Prolong Gold (Invitrogen) and kept 24hours at RT in dark. The slides were then stored at 4°C for 48hours before imaged. Images were obtained with a STED Expert Line Microscope from Abberior Instruments with a 100x oil objective (NA=1.4) as described in Pooryasin et al.[69]

Pupal brain culture and Live-Imaging

For all ex-*vivo* live imaging experiments, pupal or adult brain was carefully dissected out of the pupal case or the surrounding exoskeleton respectively. The resultant eye-brain complexes were mounted in 0.4% dialyzed low-melting agarose in a modified culture medium as described in Özel et al.[70] We used double sided tapes cut into 1inch x 1inch small squares as coverslips. Since all our developmental imaging were done after P48, we used Hydroxyecdysone free culture media. To fully expose DCN branch projection patterns, the pupae were mounted posterior side up. Live imaging was performed at room temperature using a Leica TCS SP8 X confocal microscope with a resonant scanner, using 63X water objective (NA=1.2), and optimized settings of minimal white laser excitation and crosstalk avoiding SP detector emission windows. White laser excitation was set to 488 nm for GFP, 554 nm for tdTomato signal acquisitions.

Trans-tango and activity-dependent GRASP

Trans-tango was performed with DCN-specific ato-Gal4-14a[25] and M-DCN-Gal4[28] whereas GRASP experiment was performed with DCN-specific ato-LexA. Trans-tango flies were raised both at 18°C and 25°C to optimize the dissection conditions. 7 days old flies raised at 25°C showed dense connectivity pattern. The number of postsynaptic neurons was counted manually from their cell bodies using the "surface" tool in IMARIS, including all cell bodies with weak or strong labelling to reveal all potential connections. Since

Please cite this article in press as: Dutta et al., EGFR-dependent suppression of synaptic autophagy is required for neuronal circuit development, Current Biology (2022), https://doi.org/10.1016/j.cub.2022.12.039

postsynaptic partner labeling by Trans-tango is age-dependent, 3-days old flies reared at 25°C were dissected for sparse labeling to reveal the identity of post-synaptic cell types connected to M-DCNs.

For activity-dependent GRASP experiments, to activate DCNs, freshly eclosed flies were transferred to 25°C incubator with 12–12hours light-dark cycle for 5 days. Brains were dissected and stained with a polyclonal anti-GFP antibody to label DCN pre-synaptic sites, monoclonal anti-GFP antibody to label GRASP signal, and polyclonal anti-CD4 antibody to label postsynaptic neurons as described in Kiral et al.[35] See the key resources table for the list and concentration of primary and secondary antibodies used in this study.

Buridan's paradigm assay

Fly navigation behavior was tested in a Buridan's paradigm arena as described in Linneweber et al.[28] using flies grown in a 12/12 hours light–dark cycle at 50% relative humidity. The arena consists of a round platform of 117 mm in diameter, surrounded by a water-filled moat and placed inside a uniformly illuminated white cylinder. The light was produced by four circular fluorescent tubes (Osram, L 40w, 640 C circular cool white) powered by an Osram Quicktronic QT-M 1 × 26–42. The fluorescent tubes were located outside of a diffuser (DeBanier, Belgium, 2090051, Kalk transparent, 180 g, white) positioned 147.5 mm away from the arena center. The temperature on the platform was kept constant at 25 °C. 30 mm-wide stripes of black cardboard were placed on opposing sides inside of the diffuser and served as visual targets. The retinal size of the visual object depends on the position of the fly on the platform. In this arena it ranges from 8.4° to 19.6° in width (11.7° in the center of the platform). Similar behavioral setup without the stripes were used for testing behavioral activity in absence of any visual stimuli. Fly tracks were analyzed using CeTrAn (coulomb) and custom-written python code from Linneweber et al.[28] 25 partially overlapping behavioral parameters were evaluated as follows.

Measures of overall activity

Number of walks: The number of times a fly walks from one stripe to the other. The fly needs to be on both ends near the edge more than 80% of the platform radius. Pause duration (s): Median duration of pauses in seconds. Distance travelled (mm/min): Total distance travelled per minute. Relative time moving: ratio of moving vs. not moving over the entire length of the fly track. Activity time (s): Time active per minute in seconds. Speed (mm/s): Division of the distance travelled by time in mm/s. The reported value is the median speed of each fly. Movements exceeding 50mm/s are excluded in the median speed calculation. Number of pauses: number of pauses per minute. Activity bouts (s): Median duration of bouts of activity in seconds

Measures of movement angles or location independent of visual cue

Meandering (degrees/mm): Measurement of the tortuosity (twistedness) of the track, calculated as Turning Angle divided by the speed. Shown as median value in degrees/mm. Turning angle (degrees): Median angle of all turns a fly does in the arena. Centrophobism while moving: The arena is divided in an inner and outer ring of equal size. The ratio of time spend in the inner and outer ring is calculated. 1 signifies the fly has spent all its time in the outer part of the arena. -1 signifies the fly was at all times in the inner part of the arena. 0 would signifiy an equal distribution between inner and outer part of the arena: Only parts of the track while the fly is moving count to the calculation. Centrophobism while stationary: Only parts of the track while the fly is not moving count to the calculation. Center deviation while moving: Deviation away from the center of the platform. Values given in percent of the radius. Only parts of the track while the fly is moving count to the calculation. Center deviation while stationary: Only parts of the track while the fly is not moving count to the calculation.

Measures of angles or location relative to visual cue

Absolute angle deviation: Deviation angle from the path a fly walks away from the direction of the closest stripe. Direction does not matter. Median of all deviations is reported in degrees. Stripe deviation while moving: Deviation away from the idealized line through the middle of the stripe. Direction towards right or left does matter. Values given in percent of the radius. Stripe deviation while stationary: Deviation away from the idealized line through the middle of the stripe. Direction towards right or left does matter. Values given in percent of the radius. Absolute stripe deviation while moving: Deviation away from the idealized line through the middle of the stripe. Direction towards right or left does not matter. Values given in percent of the radius. Absolute stripe deviation while stationary: Deviation away from the idealized line through the middle of the stripe. Direction towards right or left does not matter. Values given in percent of the radius. Angle deviation while stationary: Deviation away from the idealized line through the middle of the stripe. Direction towards right or left does not matter. Values given in percent of the radius. Angle deviation while moving: Deviation angle from the path a fly walks away from the direction of the closest stripe. Direction does matter. Median of all deviations is reported in degrees. Horizon deviation while moving: Deviation away from the idealized line perpendicular to the stripes. Direction towards top or bottom stripe does matter. Values given in percent of the radius. Horizon deviation while stationary: Deviation away from the idealized line perpendicular to the stripes. Direction towards top or bottom stripe does matter. Values given in percent of the radius. Absolute horizon deviation while moving: Deviation away from the idealized line perpendicular to the stripes. Direction towards top or bottom stripe does not matter. Values given in percent of the radius. Absolute horizon deviation while stationary: Deviation away from the idealized line perpendicular to the stripes. Direction towards top or bottom stripe does not matter. Values given in percent of the radius.

Significant differences between experiment and controls and the rescue experiment were only found for parameters affecting motility.

The three selected activity related behavioral parameters are the following:

Distance traveled (mm/min): Total distance travelled in mm per minute. Activity time (s): Time active per minute in seconds. Number of walks: The number a fly walks from one stripe to the other. The fly needs to be on both ends near the edge closer than 80% of the platform radius for a walk to count.

Please cite this article in press as: Dutta et al., EGFR-dependent suppression of synaptic autophagy is required for neuronal circuit development, Current Biology (2022), https://doi.org/10.1016/j.cub.2022.12.039

The data was statistically analyzed using the Kruskal- Wallis rank sum test and pairwise Wilcoxon rank sum test as a post-hoc test using R. (The post-hoc test was corrected with the Benjamini-Hochberg procedure to correct for multiple comparison)

QUANTIFICATION AND STATISTICAL ANALYSIS

Branch number and length analysis

For each mutant condition we used the same imaging conditions for its controls. All imaging data were analyzed and presented with Imaris 9.0.1 (Bitplane). Branch numbers were detected automatically with the filament module using identical parameters for all experimental conditions (largest dendrite diameter: 3.0 μm, thinnest dendrite diameter: 0.2 μm). The resultant branch numbers were then recorded directly from the statistics tab of filament module and normalized it to the total number of axons per optic lobe. Any inconsistencies in automatic detection of branches were checked and corrected manually. Branch lengths were calculated manually using the "automatic placement'' version of the filament module to calculate the 3D length of all branches. Intersection of axon shaft-primary branch were considered as the starting node and a filament was drawn till the respective branch tip. The resultant values of branch lengths were taken and recorded directly from the statistics tab of the filament module. Graph generation and statistical analyses were done using GraphPad Prism 8.2.0

Synapse number analysis

For each mutant condition we used the same imaging conditions for its controls. All imaging data were analyzed and presented with Imaris 9.0.1 (Bitplane). For synapse number analysis, CD4-tomato channel was used to generate surfaces for DCN axonal branches. Brp-positive puncta inside the surface were filtered using the masking function and were detected manually for individual branches. To obtain synapse distribution, we normalized the number of Brp-positive puncta inside individual DCN branch to the respective branch length which was calculated using the filament module as discussed above. Graph generation and statistical analyses were done using GraphPad Prism 8.2.0

Live tracing of molecules in branches

For each mutant condition we used the same imaging conditions for its controls. All imaging data were analyzed and presented with Imaris 9.0.1 (Bitplane) and the background noise was corrected with the threshold > background subtraction with a filter width of 60um in Imaris. GFP positive puncta were then tracked individually and manually for all the branches marked in CD4 channel over time and recorded. To obtain a distribution, we normalized the number of GFP-positive puncta inside individual DCN branch to the respective branch length which was calculated using the filament module. Graph generation and statistical analyses were done using GraphPad Prism 8.2.0

mCherry/pHluorin intensity and volume analysis

For each mutant condition we used the same imaging conditions for its controls. For each mutant condition we used the same imaging conditions for its control(s). Intensity analysis was performed using the surface module of Imaris 9.0.1 (Bitplane). All mCherry positive BrpD3 puncta were used to generate surface using the same threshold parameters (Diameter of largest spere which fits into the object=0.700 um; surface detail=0.481um) for experiments and controls. Volume or Mean intensity of the individual red channel (mCherry) to green channel (pHluorin) within each surface were recorded. Graph generation and statistical analyses were done using GraphPad Prism 8.2.0.

Colocalization analysis

For each mutant condition we used the same imaging conditions for its controls. All imaging data were analyzed and presented with Imaris 9.0.1 (Bitplane). For colocalization analysis, CD4-tomato channel was used to generate surfaces for DCN axonal branches. Brp-positive puncta (green channel) and the Rab7 puncta (red channel) inside the surface were filtered using the ''masking'' tool of surface module. All co-localization events were quantified manually on slice-by-slice basis for the entire z-stack in 2D. Only discernible individual compartments were counted. Full correlation (as indicated in Figure S7A′) were given a score of 1 (''yes'' colocalization) whereas 0 (''no'' colocalization) if not. To obtain the fraction of colocalized events, the total number of colocalized Brp-Rab7 puncta were divided by the total BrpD3 puncta per axon. Graph generation and statistical analyses were done using GraphPad Prism 8.2.0.

Statistical analysis

Statistical comparison of two groups was performed with non-parametric Mann-Whitney test (T-test). Statistical comparison of more than two groups was performed with non-parametric Kruskal-Wallis test and corrected for multiple comparisons with Dunn's as a post-hoc test. All significance values are denoted on the graphs and in their respective legends. Graph generation and statistical analyses were done using GraphPad Prism 8.2.0.